complex gel containing phenylboronic acid. Anal Chem 1996; 8(5):823–8.
[24] Bouriotis V, Galpin IJ, Dean PDG. Application of immobilized phenylboronic acids as supports for group-specific ligands in the affinity chromatography of enzymes. J Chromatogr 1981;210: 267–78.
[25] Gould BJ, Hall PM, Cook JGH. Measurement of glycosylated haemoglobins using an affinity chromatography method. Clin Chim Acta 1982;125:41–8.
[26] Vidal P, Deckert T, Hansen B, Welinder BS. High-performance liquid chromatofocusing and column affinity chromatography of in vitro ^{14}C-glycated human serum albumin: demonstration of a glycation-induced anionic heterogeneity. J Chromatogr A 1989;476: 467–75.
[27] Ishihara K, Ueda T, Nakabayashi N. Preparation of phospholipid polymers and their properties as polymer hydrogel membranes. Polym J 1990;22:355–60.
[28] Chen T, Embree HD, Brown EM, Taylor MM, Payne GF. Enzyme-catalyzed gel formation of gelatin and chitosan: potential for in situ applications. Biomaterials 2003;24:2341–831.
[29] Ivanova AE, Larssonb H, Galaeva IY, Mattiasson B. Synthesis of boronate-containing copolymers of *N*,*N*-dimethylacrylamide, their interaction with poly(vinyl alcohol) and rheological behavior of the gels. Polymer 2004;45:2495–505.
[30] Kishida M, Akita H. Synthesis of rosavin and its analogues based on a mizoroki-heck type reaction. Tetrahedron: Asymmetry 2005;16: 2625–30.
[31] Kitano S, Koyama Y, Kataoka K, Okano T, Sakurai Y. A novel drug delivery system utilizing a glucose responsive polymer complex between poly(vinyl alcohol) and poly(*N*-vinyl-2-pyrrolidone) with a phenylboronic acid moiety. J Control Release 1992;19:161–70.
[32] Shiino D, Murata Y, Kubo A, Kim YJ, Kataoka K, Koyama Y, et al. Amine containing phenylboronic acid gel for glucose-responsive insulin release under physiological pH. J Control Release 1995; 37:269–76.
[33] Shiino D, Murata Y, Kataoka K, Koyama Y, Yokoyama M, Okano T, et al. Preparation and characterization of a glucose-responsive insulin-releasing polymer device. Biomaterials 1994;15:121–8.
[34] Ziaie B, Baldi A, Lei M, Gu Y, Siegel RA. Hard and soft micromachining for BioMEMS: review of techniques and examples of applications in microfluidics and drug delivery. Adv Drug Deliv Rev 2004;56:145–72.
[35] Sawada S, Sakaki S, Iwasaki Y, Nakabayashi N, Ishihara K. Suppression of the inflammatory response from adherent cells on phospholipid polymers. J Biomed Mater Res A 2003;64:411–6.
[36] Mooney D, Hansen L, Vacanti J, Langer R, Farmer S, Ingber D. Switching from differentiation to growth in hepatocytes: Control by extracellular matrix. J Cell Physiol 1992;151:497–505.
[37] Chen CS, Mrksich M, Huang S, Whitesides GM, Ingber DE. Micropatterned surfaces for control of cell shape, position, and function. Biotechnol Prog 1998;14:356–63.
[38] Konno T, Akita K, Kurita K, Ito Y. Formation of embryoid bodies by mouse embryonic stem cells on plastic surfaces. J Biosci Bioeng 2005;100:88–93.

Phosphorylation of GSK-3β by cGMP-dependent protein kinase II promotes hypertrophic differentiation of murine chondrocytes

Yosuke Kawasaki,[1] Fumitaka Kugimiya,[1] Hirotaka Chikuda,[1] Satoru Kamekura,[1] Toshiyuki Ikeda,[1] Naohiro Kawamura,[1] Taku Saito,[1] Yusuke Shinoda,[1] Akiro Higashikawa,[1] Fumiko Yano,[1] Toru Ogasawara,[1] Naoshi Ogata,[1] Kazuto Hoshi,[1] Franz Hofmann,[2] James R. Woodgett,[3] Kozo Nakamura,[1] Ung-il Chung,[1] and Hiroshi Kawaguchi[1]

[1]Sensory and Motor System Medicine, Faculty of Medicine, University of Tokyo, Tokyo, Japan. [2]Institut für Pharmakologie und Toxikologie, Technische Universität München, Munich, Germany. [3]Samuel Lunenfeld Research Institute, Toronto, Ontario, Canada.

cGMP-dependent protein kinase II (cGKII; encoded by *PRKG2*) is a serine/threonine kinase that is critical for skeletal growth in mammals; in mice, cGKII deficiency results in dwarfism. Using radiographic analysis, we determined that this growth defect was a consequence of an elongated growth plate and impaired chondrocyte hypertrophy. To investigate the mechanism of cGKII-mediated chondrocyte hypertrophy, we performed a kinase substrate array and identified glycogen synthase kinase–3β (GSK-3β; encoded by *Gsk3b*) as a principal phosphorylation target of cGKII. In cultured mouse chondrocytes, phosphorylation-mediated inhibition of GSK-3β was associated with enhanced hypertrophic differentiation. Furthermore, cGKII induction of chondrocyte hypertrophy was suppressed by cotransfection with a phosphorylation-deficient mutant of GSK-3β. Analyses of mice with compound deficiencies in both protein kinases ($Prkg2^{-/-}Gsk3b^{+/-}$) demonstrated that the growth retardation and elongated growth plate associated with cGKII deficiency were partially rescued by haploinsufficiency of *Gsk3b*. We found that β-catenin levels decreased in $Prkg2^{-/-}$ mice, while overexpression of cGKII increased the accumulation and transactivation function of β-catenin in mouse chondroprogenitor ATDC5 cells. This effect was blocked by coexpression of phosphorylation-deficient GSK-3β. These data indicate that hypertrophic differentiation of growth plate chondrocytes during skeletal growth is promoted by phosphorylation and inactivation of GSK-3β by cGKII.

Introduction

Skeletal growth is achieved by endochondral ossification in the growth plate cartilage, with orderly columnar arrays of resting, proliferative, and hypertrophic zones of chondrocytes. During the process, chondrocytes undergo proliferation, hypertrophic differentiation, and apoptosis, each of which is regulated by distinct molecular signaling systems (1). Among them, C-type natriuretic peptide (CNP; encoded by *Nppc*), a humoral factor that can regulate a variety of homeostatic processes by binding the membrane-bound guanylyl cyclase–coupled receptor B (GC-B; encoded by *Npr2*), has been shown to play important roles in skeletal growth, because mice deficient in either gene exhibit impaired skeletal growth (2, 3). Loss-of-function mutations in *Npr2* also show dwarfism in patients known as acromesomelic dysplasia, type Maroteaux (4), demonstrating the importance of CNP/GC-B signaling in the skeletal growth of humans as well. This signaling causes the intracellular accumulation of cGMP, which then activates cGMP-dependent protein kinases (cGKs) (5). In mammalian cells, there are 2 cGK isoforms, cGKI and cGKII (encoded by *Prkg1* and *Prkg2*, respectively), which show distinct distributions and functions (6, 7). Although both are expressed in growth plate cartilage, $Prkg2^{-/-}$ mice show postnatal dwarfism with about 20%–30% reduction in the length of limbs and trunk (6), while $Prkg1^{-/-}$ mice show a normal skeleton (8), indicating that only cGKII is indispensable for skeletal growth.

cGKII is a membrane-bound serine/threonine kinase with a cGMP-binding domain and a catalytic domain in the C terminus (7). In addition to growth retardation resulting from cGKII deficiency in mice, our previous positional cloning analysis identified a deletion in *Prkg2*, the rat gene encoding cGKII, in the Komeda miniature rat Ishikawa (KMI), a naturally occurring mutant rat, which also exhibited dwarfism with 20%–30% shorter long bones and vertebrae (9). The deletion resulted in a frame shift and a premature stop codon, predicting a truncated cGKII protein that lacks the kinase domain (cGKII-Δkinase). KMI rats show an elongated growth plate, whose height is about 2.5-fold that of WT littermates. This is caused by the existence of an abnormal intermediate layer between the proliferative and hypertrophic zones with accumulation of few proliferative or hypertrophic chondrocytes, which indicates that the kinase activity of cGKII is necessary for

Nonstandard abbreviations used: ALP, alkaline phosphatase; Bad, BCL2-antagonist of cell death; cdc25, cell division cycle 25 homolog; cGK, cGMP-dependent protein kinase; cGKII-Δkinase, truncated cGKII protein that lacks the kinase domain; CNP, C-type natriuretic peptide; COL10, type X collagen; GC-B, guanylyl cyclase–coupled receptor B; GSK-3β, glycogen synthase kinase-3β; $GSK\text{-}3\beta^{S9A}$, phosphorylation-deficient mutant of GSK-3β with a serine-to-alanine substitution; PLK, polo-like kinase; p90RSK, 90-kDa ribosomal protein S6 kinase; PTH, parathyroid hormone; PTHrP, parathyroid hormone–related protein; TCF, T cell factor; VASP, vasodilator-stimulated phosphoprotein.

Conflict of interest: The authors have declared that no conflict of interest exists.

Citation for this article: *J. Clin. Invest.* **118**:2506–2515 (2008). doi:10.1172/JCI35243.

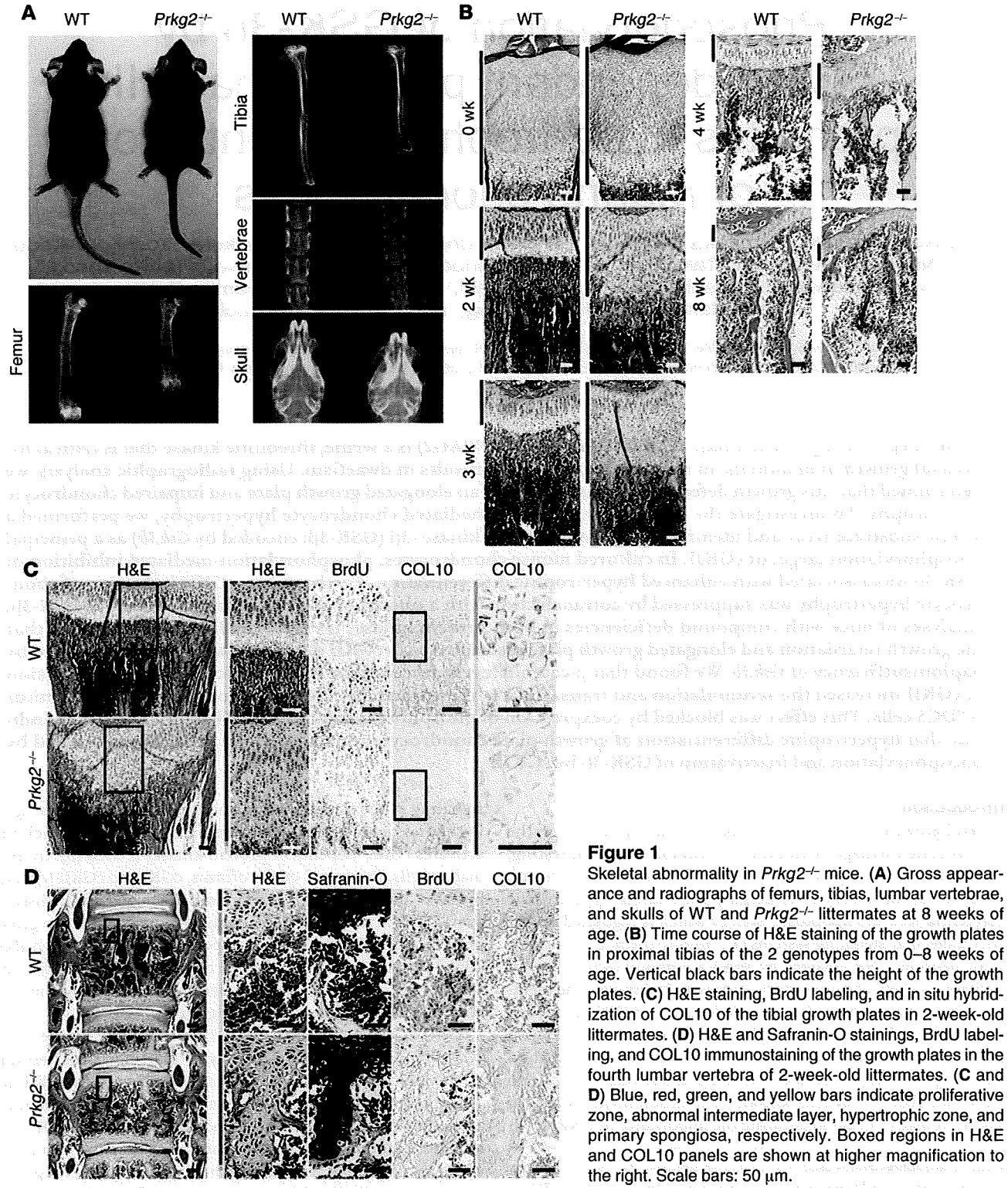

Figure 1
Skeletal abnormality in *Prkg2*$^{-/-}$ mice. (**A**) Gross appearance and radiographs of femurs, tibias, lumbar vertebrae, and skulls of WT and *Prkg2*$^{-/-}$ littermates at 8 weeks of age. (**B**) Time course of H&E staining of the growth plates in proximal tibias of the 2 genotypes from 0–8 weeks of age. Vertical black bars indicate the height of the growth plates. (**C**) H&E staining, BrdU labeling, and in situ hybridization of COL10 of the tibial growth plates in 2-week-old littermates. (**D**) H&E and Safranin-O stainings, BrdU labeling, and COL10 immunostaining of the growth plates in the fourth lumbar vertebra of 2-week-old littermates. (**C** and **D**) Blue, red, green, and yellow bars indicate proliferative zone, abnormal intermediate layer, hypertrophic zone, and primary spongiosa, respectively. Boxed regions in H&E and COL10 panels are shown at higher magnification to the right. Scale bars: 50 μm.

hypertrophic differentiation of growth plate chondrocytes (9). To investigate the mechanism underlying cGKII kinase activity in chondrocyte hypertrophy, in the present study we performed a screen of its potential phosphorylation targets and identified glycogen synthase kinase–3β (GSK-3β; encoded by *Gsk3b*) as a significant phosphorylation target of cGKII. Because the phosphorylation of GSK-3β at Ser9 is known to cause its inactivation (10), we further examined the functional involvement of GSK-3β in the cGKII-induced hypertrophic differentiation of chondrocytes and investigated the underlying mechanism. Our results demonstrated that cGKII promotes chondrocyte hypertrophy and skeletal growth through phosphorylation and inactivation of GSK-3β.

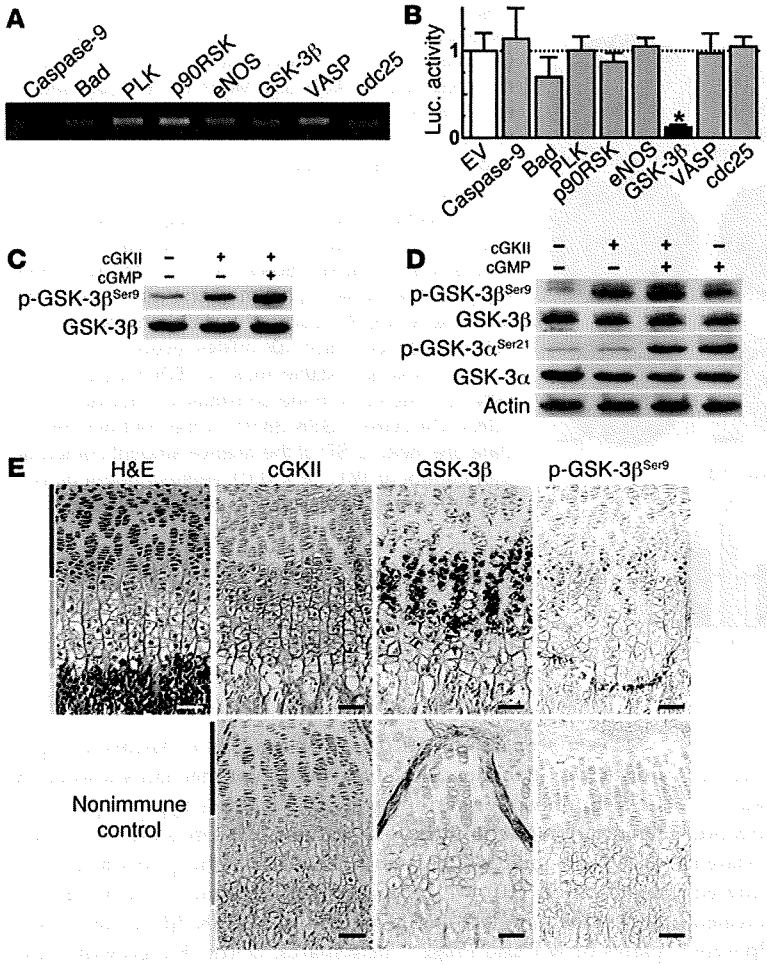

Figure 2
Identification of GSK-3β as a principal phosphorylation target of cGKII during chondrocyte hypertrophy. (**A**) RT-PCR of 8 candidate genes that were identified by the serine/threonine kinase substrate array (Supplemental Table 1) in cultured ATDC5 cells in the prehypertrophic or hypertrophic differentiation stage. (**B**) COL10 promoter activity, as assessed by transfection of the 8 candidate genes or the empty vector (EV) in HuH-7 cells with the luciferase reporter gene construct containing a cloned 4.5-kb promoter fragment of COL10. Data are mean ± SD fold change relative to empty vector. $^*P < 0.01$ versus control. (**C**) In vitro kinase assay of the phosphorylation of recombinant GSK-3β at Ser9 by recombinant cGKII with or without cGMP. Proteins were incubated in the presence of ATP, and the reaction products were analyzed by IB using the same antibody to Ser9-phosphorylated GSK-3β (p-GSK-3β^{Ser9}) as that used in Supplemental Table 1. (**D**) Phosphorylation of endogenous GSK-3β at Ser9 and GSK-3α at Ser21 by cGKII with or without cGMP in ATDC5 cells. Whole-cell lysates were incubated with recombinant cGKII or cGMP in the presence of ATP, and the reaction products were analyzed as in **C**. (**E**) Localization of cGKII, total GSK-3β, and Ser9-phosphorylated GSK-3β, as assessed by immunohistochemistry in the growth plate of proximal tibia in a 2-week-old mouse. Specific stainings were confirmed by immunohistochemistry by respective nonimmune serums (nonimmune control). Blue, green, and yellow bars indicate proliferative zone, hypertrophic zone, and primary spongiosa, respectively. Scale bars: 50 μm.

Results

Growth plate abnormality in Prkg2$^{-/-}$ mice. *Prkg2$^{-/-}$* mice showed postnatal dwarfism with short limbs and trunk compared with WT littermates (Figure 1A), as previously reported (6). Radiographic analysis at 8 weeks of age revealed that the lengths of femur, tibia, and vertebra, which are known to be primarily formed through endochondral ossification, were shorter in *Prkg2$^{-/-}$* mice. The longitudinal length of the *Prkg2$^{-/-}$* skull was also shorter, while the width was comparable to WT. This finding is probably attributable to 2 types of the skull growth via endochondral ossification and intramembranous ossification (11), although this needs to be further investigated. The time course of histological observation of the tibial growth plate revealed that the height was greater in *Prkg2$^{-/-}$* than WT mice from 2 to 4 weeks after birth but was restored to a level comparable to that of WT mice by 8 weeks of age (Figure 1B). As previously observed in KMI rats (9), growth plate elongation during these ages was caused by an abnormal intermediate layer between the proliferative and hypertrophic zones, with accumulation of few proliferative or hypertrophic chondrocytes, as determined by BrdU uptake and expression of type X collagen (COL10), respectively (Figure 1C). The growth plate of the *Prkg2$^{-/-}$* vertebral bones also contained the abnormal intermediate layer, which was intermittently focal in the elongated growth plate (Figure 1D). These results indicate that cGKII is necessary for hypertrophic differentiation of growth plate chondrocytes during endochondral ossification for longitudinal growth of limbs and trunk not only in rats, but also in mice.

Phosphorylation targets of cGKII in chondrocyte hypertrophy. To investigate the mechanism underlying cGKII activity in hypertrophic differentiation of chondrocytes, we performed a screen of its phosphorylation targets by in vitro kinase assay using a serine/threonine kinase substrate array. From 87 candidate peptides containing serine/threonine phosphorylation sites, we identified 8 substrates that were most strongly phosphorylated by cGKII: caspase-9, BCL2-antagonist of cell death (Bad), polo-like kinase (PLK), 90-kDa ribosomal protein S6 kinase (p90RSK), eNOS, GSK-3β, vasodilator-stimulated phosphoprotein (VASP), and cell division cycle 25 homolog (cdc25) (Supplemental Table 1; supplemental material available online with this article; doi:10.1172/JCI35243DS1). All of these molecules were confirmed to be expressed in mouse chondrogenic ATDC5 cells in the prehypertrophic or hypertrophic differentiation stage (Figure 2A). However, a luciferase reporter assay revealed that GSK-3β markedly suppressed COL10 promoter activity, while none of the other candidates had a significant effect (Figure 2B). These data suggest that GSK-3β might be functionally involved in chondrocyte hypertrophy, although involvement of the other factors cannot be ruled out. Direct phosphorylation of recombinant GSK-3β at Ser9, the crucial site for inactivation of GSK-3β (10), by recombinant cGKII protein was confirmed by in vitro kinase assay using the same antibody as the screening array above, and the phos-

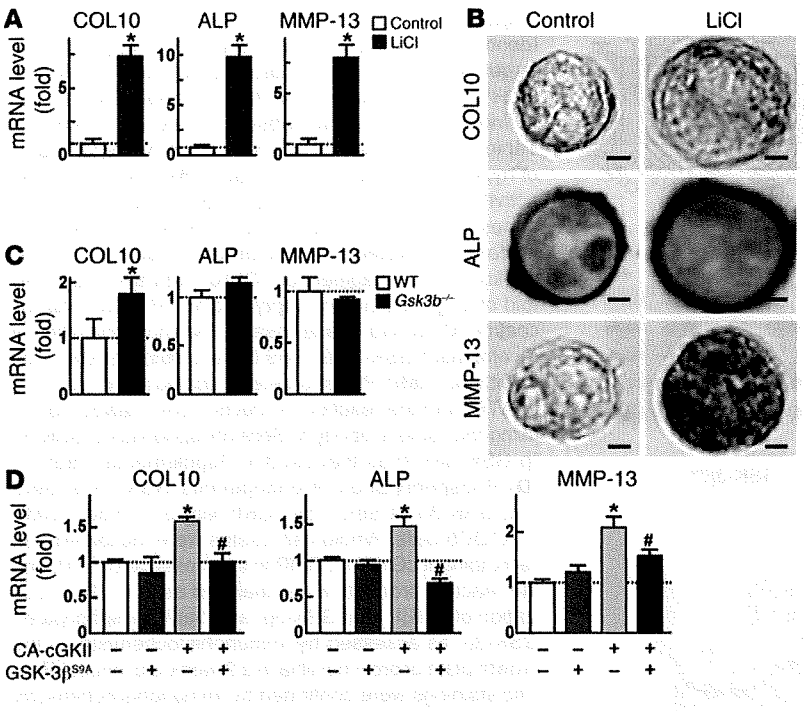

Figure 3
Regulation of chondrocyte hypertrophy by GSK-3β. (**A**) Effects of LiCl on mRNA levels of the hypertrophic markers COL10, ALP, and MMP-13, as assessed by real-time RT-PCR in ATDC5 cells cultured in 3-dimensional alginate beads. (**B**) Effects of LiCl on the hypertrophic markers, as assessed by immunocytochemistry in primary costal chondrocytes cultured in 3-dimensional alginate beads. For morphological comparison, sections of the representative colonies containing 4 cells were selected. Scale bars: 10 μm. (**C**) mRNA levels of the hypertrophic markers, as assessed by real-time RT-PCR in cultured costal chondrocytes from WT and *Gsk3b*$^{+/-}$ mice. (**D**) mRNA levels of the hypertrophic markers in stable lines of ATDC5 cells retrovirally transfected with the constitutively active form of cGKII (CA-cGKII), GSK-3β^{S9A}, or the control GFP (–). Data are mean ± SD of the relative amount compared with control or WT. $^{*}P < 0.01$ versus control or WT. $^{\#}P < 0.01$ versus constitutively active cGKII alone.

phorylation was enhanced by the addition of cGMP (Figure 2C). Furthermore, endogenous GSK-3β in cell lysates of ATDC5 cells was phosphorylated at Ser9 by recombinant cGKII protein, which was further enhanced by the addition of cGMP. On the other hand, GSK-3α, the closely related isoform of GSK-3β, was not phosphorylated by cGKII, nor were protein levels of GSK-3β and GSK-3α altered by cGKII or cGMP (Figure 2D). Immunohistochemistry revealed that cGKII, total GSK-3β, and Ser9-phosphorylated GSK-3β were colocalized in prehypertrophic chondrocytes of the growth plate, implicating the interaction of these molecules in vivo as well (Figure 2E). Compared with the respective nonimmune controls, the localization of Ser9-phosphorylated GSK-3β appeared to be restricted to those cells that also produced cGKII, whereas total GSK-3β was more broadly distributed, which supports the notion that cGKII is an important regulator of GSK-3β phosphorylation.

Regulation of chondrocyte hypertrophy by GSK-3β. In the 3-dimensional cultures of ATDC5 cells and primary costal chondrocytes in alginate beads, LiCl, a selective inhibitor of GSK-3β, stimulated the expression of chondrocyte hypertrophic differentiation markers COL10, alkaline phosphatase (ALP), and MMP-13 and induced morphological hypertrophy of the cells (Figure 3, A and B). COL10 expression also increased in cultured primary costal chondrocytes from *Gsk3b*$^{+/-}$ mice compared with WT chondrocytes, while ALP and MMP-13 levels were comparable between the genotypes (Figure 3C). Introduction of a constitutively active allele of cGKII into ATDC5 cells stimulated expression of hypertrophic markers, and this was attenuated by the cointroduction of a phosphorylation-deficient mutant of GSK-3β with a serine-to-alanine substitution (GSK-3β^{S9A}), which is known to have constitutive activity (Figure 3D). These data demonstrated that Ser9 phosphorylation of GSK-3β is necessary for the induction of chondrocyte hypertrophy by cGKII. The GSK-3β^{S9A} introduction alone altered none of the 3 markers (Figure 3D), which indicates that an endogenous GSK-3β level was sufficient for the suppression of chondrocyte hypertrophy in this culture system.

Mechanism underlying cGKII/GSK-3β signaling in chondrocyte hypertrophy. We further examined the molecular mechanism whereby GSK-3β phosphorylation by cGKII regulates hypertrophic differentiation of chondrocytes. Because GSK-3β is known to be a negative regulator of β-catenin through its phosphorylation and degradation (10), we compared the localization of β-catenin, Ser9-phosphorylated GSK-3β, and total GSK-3β in the growth plates of WT and *Prkg2*$^{-/-}$ littermates. In the WT growth plate, β-catenin as well as both GSK-3β proteins were localized mainly in the cytoplasm of prehypertrophic chondrocytes (Figure 4A). cGKII deficiency caused similar decreases in β-catenin and Ser9-phosphorylated GSK-3β levels with little effect on the total GSK-3β level in the abnormal intermediate layer. In cultured ATDC5 cells, cGKII induced cytosolic accumulation of β-catenin after stimulation by 8-bromo-cGMP, while cGKII-Δkinase had a minimal effect (Figure 4B). Overexpression of constitutively active cGKII enhanced the promoter activity of the β-catenin target T cell factor (TCF), which was markedly suppressed by cotransfection of GSK-3β^{S9A} (Figure 4C). Again, GSK-3β^{S9A} alone did not have an effect, which indicates that an endogenous GSK-3β level is sufficient for β-catenin suppression. We next examined the involvement of a scaffolding peptide, Axin, which is known to associate with GSK-3β and promotes effective phosphorylation and degradation of β-catenin under conditions of Wnt stimulation (10). IP/IB analysis using HEK293 cells transfected with Myc-tagged Axin and cGKII revealed that cGKII formed a complex with Axin and phosphorylated GSK-3β not only in the whole-cell lysates, but also in the IP with Axin, suggesting some interaction between Ser9 phosphorylation and coupling with Axin in regulation of GSK-3β by cGKII (Figure 4D).

In our previous study, we showed that cGKII caused attenuation of Sox9 transcriptional function through inhibition of nuclear entry (9). Because Sox9 is known not only to induce chondrogenic differentiation of mesenchymal cells, but also to prevent hypertrophic differentiation of chondrocytes (12), this may contribute

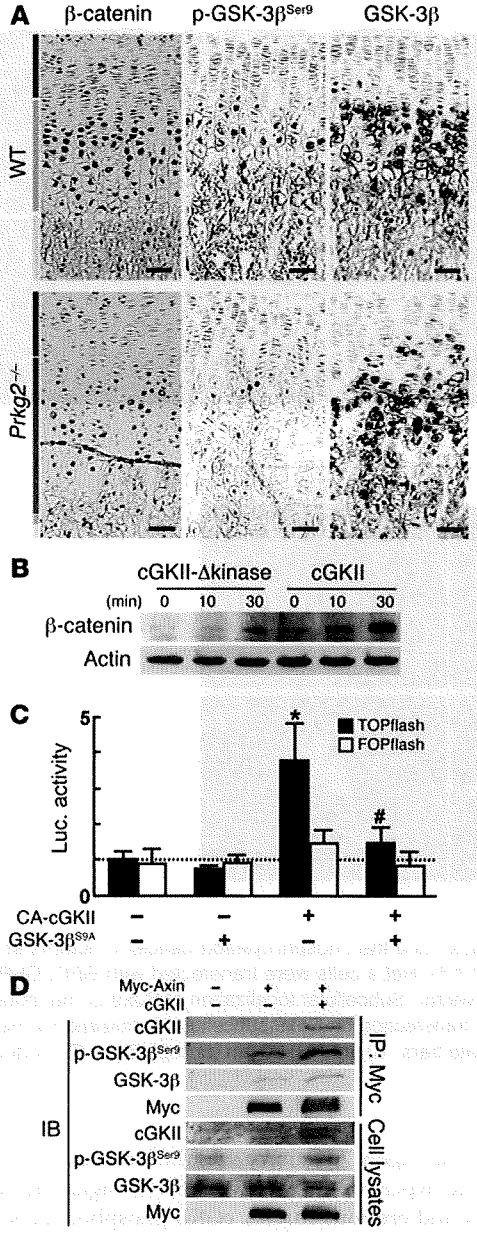

Figure 4

Mechanism underlying cGKII/GSK-3β signaling in chondrocyte hypertrophy. (**A**) Localization of β-catenin, Ser9-phosphorylated GSK-3β, and total GSK-3β, as assessed by immunohistochemistry in the growth plates of the proximal tibias of WT and *Prkg2*$^{-/-}$ mice at 2 weeks of age. Blue, red, green, and yellow bars indicate proliferative zone, abnormal intermediate layer, hypertrophic zone, and primary spongiosa, respectively. Scale bars: 50 μm. (**B**) Time course of β-catenin protein level after stimulation by 8-bromo-cGMP, as assessed by IB in the cytosolic fraction of ATDC5 cells with retroviral introduction of cGKII or cGKII-Δkinase. (**C**) Promoter activity of the β-catenin target TCF, as assessed by luciferase (Luc) assay using TOPflash and FOPflash reporter plasmids in HEK293 cells transfected with constitutively active cGKII, GSK-3β^{S9A}, or the control GFP (–). Data are mean ± SD fold change compared with control (–/–). $^{*}P < 0.01$ versus control. $^{\#}P < 0.01$ versus constitutively active cGKII alone. (**D**) Physical association of cGKII and GSK-3β with Axin by IP/IB analysis. HEK293 cells were transfected with Myc-tagged Axin (Myc-Axin) and/or cGKII, and an aliquot of the cell lysates underwent IP with the high-affinity anti–c-Myc antibody–coupled agarose as described in Methods. The IP (Myc) or the whole-cell lysates underwent IB with an antibody to cGKII, Ser9-phosphorylated GSK-3β, GSK-3β, or Myc.

to the mechanism whereby cGKII promotes chondrocyte hypertrophy. However, inhibition of Sox9 nuclear entry by cGKII was independent of phosphorylation of Sox9 itself, because cGKII inhibited not only the nuclear entry of the WT Sox9, but also that of the phosphorylation-deficient Sox9 mutants with serine-to-alanine substitutions at putative phosphorylation sites Ser64 and Ser181 (Figure 5A), which suggests that other phosphorylation targets of cGKII are important. We therefore examined the involvement of GSK-3β phosphorylation in the inhibition of Sox9 nuclear entry by cGKII. Neither addition of the GSK-3β inhibitor LiCl nor overexpression of GSK-3β^{S9A} altered cGKII-dependent inhibition of Sox9 nuclear entry, which indicates that the inhibitory effect of cGKII was independent of GSK-3β phosphorylation by cGKII (Figure 5B).

We next assessed involvement of other putative signaling systems in cGKII action on chondrocyte hypertrophy. Although Runx2 has previously been shown to be an important transcription factor that induces hypertrophic differentiation of chondrocytes (13), its expression was visible in the abnormal intermediate layer of the *Prkg2*$^{-/-}$ growth plate (Supplemental Figure 1A). In addition, neither the mRNA level nor the subcellular localization of Runx2 was altered by cGKII overexpression in cultured ATDC5 cells (Supplemental Figure 1, B and C).

FGF signaling has also been shown to be important for chondrocyte differentiation and endochondral ossification in mice and humans (14). Considering that targeted overexpression of CNP in chondrocytes counteracts dwarfism in a mouse model of achondroplasia with activated FGF receptor 3 (15) and that the mutant mice exhibit an elongated growth plate similar to that of *Prkg2*$^{-/-}$ mice (16), there might be cross-talk between cGKII and FGF signaling. Because FGF signaling stimulates MAPK or STAT-1 signaling pathways, we examined the interaction of phosphorylation of Erk1, Erk2, p38 MAPK, JNK1, JNK2/3, and STAT-1. Among these, FGF-2 most strongly phosphorylated Erk1 and Erk2; however, overexpression of cGKII affected none of these in the presence or absence of FGF-2, indicating no apparent interaction between cGKII and FGF, MAPK, or STAT-1 signaling (Supplemental Figure 2A).

Partial reversal of the skeletal abnormality in Prkg2$^{-/-}$ *mice by GSK-3β insufficiency.* To test whether GSK-3β plays a role in mediating the effect of cGKII-induced skeletal growth changes in vivo, we examined the effect of genetic insufficiency of GSK-3β on the skeletal abnormality apparent in *Prkg2*$^{-/-}$ mice. Although *Gsk3b*$^{-/-}$ mice were embryonically lethal (17), *Gsk3b*$^{+/-}$ mice developed and grew normally (Supplemental Figure 3). We therefore crossed *Prkg2*$^{-/-}$ mice with *Gsk3b*$^{+/-}$ mice to generate compound *Prkg2*$^{-/-}$*Gsk3b*$^{+/-}$ mice. Radiographic analysis and total axial length measurement showed that *Prkg2*$^{-/-}$*Gsk3b*$^{+/-}$ mice exhibited partial, but significant, restoration (about 30%–40%) of the impaired skeletal growth of *Prkg2*$^{-/-}$ mice at 8, 12, and 16 weeks after birth (Figure 6, A and B). Measurement of skeletal length confirmed that the endochondral ossification of femur, tibia, humerus, ulna, vertebra, and skull were decreased by cGKII deficiency, while skull width and clavicle length — which are known to develop by endochondral and intra-

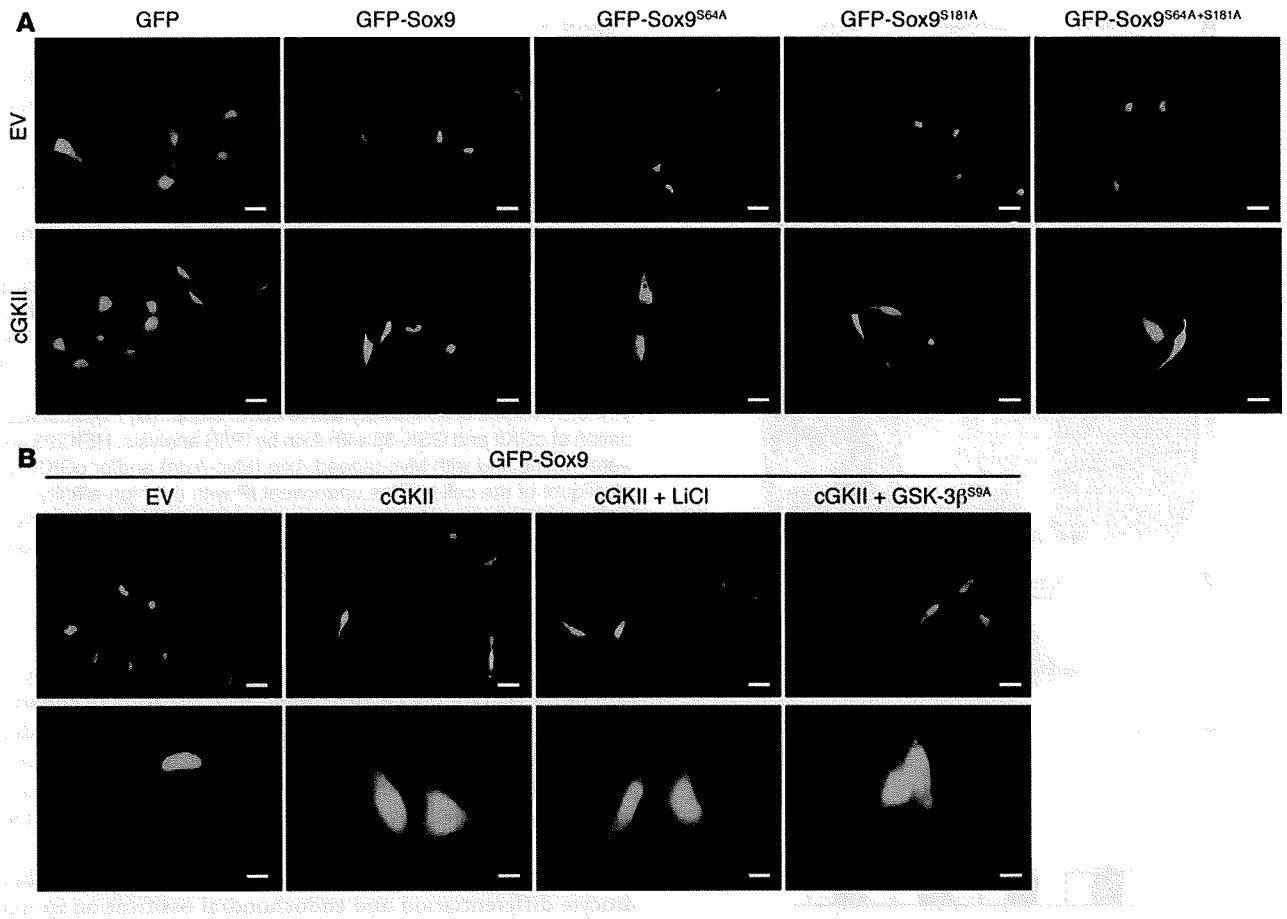

Figure 5
Subcellular localization of Sox9. (**A**) Effect of cGKII on subcellular localization of Sox9 and the phosphorylation-deficient mutants at putative phosphorylation sites at Ser64 ($Sox9^{S64A}$), Ser181 ($Sox9^{S181A}$), or both ($Sox9^{S64A+S181A}$). HeLa cells were transfected with GFP, GFP-tagged Sox9 (GFP-Sox9), or the GFP-tagged mutants in combination with cGKII or empty vector. Subcellular localization of Sox9 or the mutants was determined by a fluorescent microscope. (**B**) Effect of LiCl treatment or GSK-$3\beta^{S9A}$ transfection on Sox9 subcellular localization in HeLa cells cotransfected with GFP-tagged Sox9 in combination with cGKII or empty vector. Scale bars: 10 μm (**A**); 20 μm (**B**, top); 5 μm (**B**, bottom).

membranous ossification (11, 18) — were comparable to those of WT littermates (Figure 6C). The genetic insufficiency of GSK-3β in the *Prkg2*$^{-/-}$*Gsk3b*$^{+/-}$ mice partially, but significantly, restored the impaired skeletal growth (about 20%–40%). These findings indicate that sufficient GSK-3β function is needed for skeletal growth and endochondral ossification to be impaired by cGKII deficiency.

Further histological analyses revealed that the elongated growth plate and decreased COL10 expression in *Prkg2*$^{-/-}$ mice were also partially restored in the *Prkg2*$^{-/-}$*Gsk3b*$^{+/-}$ mice (Figure 7, A and B). In contrast, GSK-3β insufficiency did not alter skeletal growth or growth plate parameters in WT or *Prkg2*$^{+/-}$ mice, as shown in *Gsk3b*$^{+/-}$ and compound *Prkg2*$^{+/-}$*Gsk3b*$^{+/-}$ mice, respectively (Supplemental Figure 3). GSK-3β may therefore function specifically as a mediator of cGKII signaling, rather than generally in the regulation of chondrocyte hypertrophy and endochondral ossification.

Discussion

Based on our previous finding that cGKII activity is essential for the promotion of skeletal growth through hypertrophic differentiation of growth plate chondrocytes (9), the results of our present study initially identified GSK-3β as a likely substrate of this protein kinase. Figure 7C summarizes the mechanism underlying chondrocyte hypertrophy by cGKII/GSK-3β signaling based on the present and previous studies. cGKII phosphorylates GSK-3β at Ser9 and inactivates it, which may contribute to the suppression of β-catenin degradation, as previously reported (10). We and others have reported that β-catenin/TCF signaling causes stimulation of hypertrophic differentiation of chondrocytes in vitro (19–22). In addition, chondrocyte-specific inactivation of β-catenin in mice results in dwarfism with delayed hypertrophic differentiation of chondrocytes (23). Hence, the stabilization and accumulation of β-catenin by cGKII/GSK-3β signaling in chondrocytes may lead to hypertrophic differentiation, although the underlying molecular mechanism is still controversial.

Genetic rescue of impaired skeletal growth in *Prkg2*$^{-/-}$ mice by suppression of GSK-3β was significant, but incomplete (Figures 6 and 7). This might be because GSK-3β haploinsufficiency was inadequate to fully overcome the deficiency of cGKII. Indeed, cultured *Gsk3b*$^{+/-}$ chondrocytes showed higher COL10 expression, but similar ALP and MMP-13 expression, compared with WT cells, while LiCl clearly increased all hypertrophic markers in the ATDC5 cell culture (Figure 3, A and C). We cannot exclude the possibil-

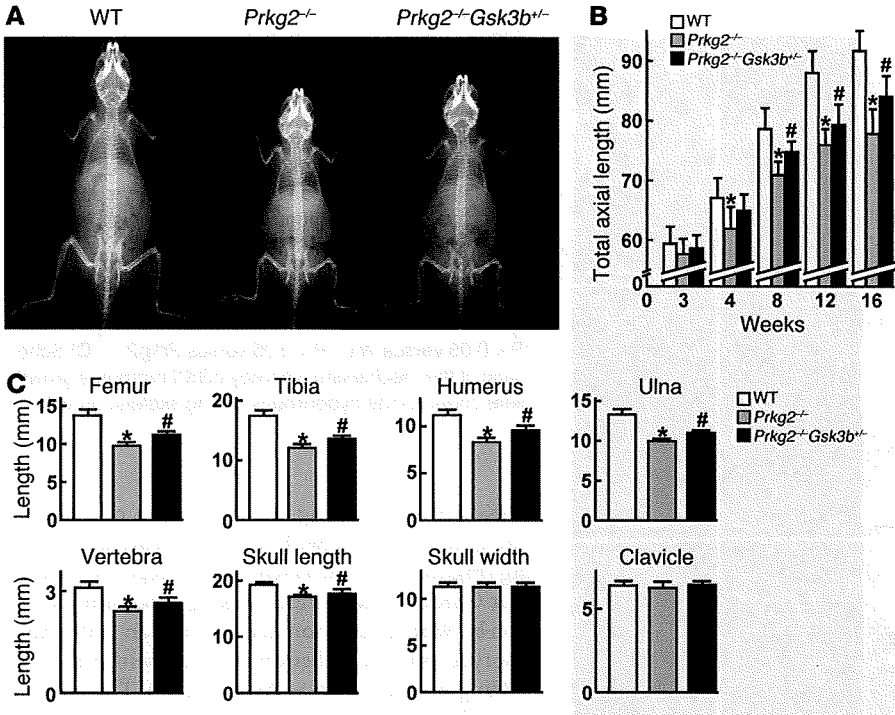

Figure 6
Genetic rescue of growth retardation in *Prkg2*$^{-/-}$ mice by GSK-3β insufficiency. (**A**) Radiographs of WT, *Prkg2*$^{-/-}$, and *Prkg2*$^{-/-}$ *Gsk3b*$^{+/-}$ littermates at 8 weeks of age. (**B**) Time course of total axial length (from nose to tail end) of the 3 genotypes from 3 to 16 weeks of age. The recovery by the GSK-3β insufficiency in the *Prkg2*$^{-/-}$ mice was 43.2%, 31.4%, and 41.9% at 8, 12, and 16 weeks, respectively. (**C**) Length of bones of the 3 genotypes at 8 weeks of age. Percent recovery was 21.7%, 18.3%, 24.3%, 16.2%, 24.3%, and 42.6% in femur, tibia, humerus, ulna, vertebra, and skull length, respectively. Data are mean ± SD for 4–9 mice per genotype. $^{*}P < 0.05$ versus WT. $^{\#}P < 0.05$ versus *Prkg2*$^{-/-}$.

ity, however, of involvement of other mechanisms in the actions of cGKII on chondrocyte hypertrophy. Although our previous study showed that cGKII phosphorylated Sox9, an inhibitor of chondrocyte hypertrophy, and suppressed its nuclear entry (9), the present study revealed that the subcellular translocation was not mediated by the phosphorylation of Sox9 itself or of GSK-3β (Figure 5). Besides Sox9 and GSK-3β, VASP and cysteine- and glycine-rich protein 2 have previously been reported as phosphorylation targets of cGKII in other types of cells (24). However, our luciferase assays failed to show regulation of COL10 transcription by either gene (Figure 2B and Supplemental Figure 2B), suggesting the existence of other phosphorylation targets of cGKII in the regulation of Sox9 translocation associated with chondrocyte hypertrophy. In addition, because Sox9 has previously been reported to physically interact with β-catenin and to compete with its binding to TCF (23), the downstream pathways of cGKII through GSK-3β and Sox9 might interact at the level of β-catenin during chondrocyte hypertrophy.

Chondrocyte hypertrophy in the growth plate is a rate-limiting step for longitudinal skeletal growth (25), because this step has been shown to be responsible for 40%–60% of endochondral ossification, with the remainder caused by chondrocyte proliferation and matrix synthesis (26). Sox9 is a representative regulator of this step, as are Runx2 (1, 13) and parathyroid hormone/parathyroid hormone–related protein (PTH/PTHrP) (1, 27), uncovered via recent advances in molecular genetics. The present study failed to find interaction between cGKII and Runx2 (Supplemental Figure 1). Although PTH/PTHrP has previously been shown to be a potent inhibitor of chondrocyte hypertrophy by the findings in deficient and transgenic mice (1, 27), our previous study revealed that neither expression levels of PTHrP and PTH/PTHrP receptor nor cAMP accumulation by PTH stimulation was altered by cGKII deficiency in chondrocytes (9). Hence, cGKII may regulate chondrocyte hypertrophy by a mechanism independent of those of Runx2 and PTH/PTHrP.

In line with the view that cGKII is a downstream mediator of CNP, *Nppc*$^{-/-}$ and *Npr2*$^{-/-}$ mice also exhibit dwarfism (2). However, unlike *Prkg2*$^{-/-}$ mice, which have an elongated growth plate with an abnormal intermediate layer, both *Nppc*$^{-/-}$ mice and *Npr2*$^{-/-}$ mice showed thinned growth plates with chondrocytes arranged in a regular columnar array. This may indicate the involvement of other signaling pathways in CNP/GC-B–mediated endochondral ossification. In fact, the intracellular accumulation of cGMP caused by CNP/GC-B signaling activates not only cGKII, but also other downstream mediators, such as cGKI, cyclic nucleotide phosphodiesterases, and cGMP-regulated ion channels (5, 28). Although no skeletal abnormality has been reported in *Prkg1*$^{-/-}$ mice (8), it would be helpful to investigate whether mice doubly deficient for cGKI and cGKII mimic the phenotype of *Nppc*$^{-/-}$ or *Npr2*$^{-/-}$ mice. In addition, targeted overexpression of CNP in growth plate chondrocytes was reported to restore the achondroplastic bone with FGF receptor 3 mutation through inhibition of the MAPK pathway (15), which we found in the present study to be unrelated to cGKII (Supplemental Figure 2A). Furthermore, cGKII functions as an effector of cGMP that is activated not only by CNP, but also by nitric oxide and other types of natriuretic peptides (5, 7, 28). Although the fact that CNP was unable to affect chondrocyte differentiation of skeletal growth in the absence of cGKII either in vitro or in vivo indicates a crucial role of cGKII in CNP signaling (29), CNP and cGKII are unlikely to function with a one-to-one correspondence during endochondral ossification.

The abnormal elongation of the *Prkg2*$^{-/-}$ mouse growth plate was apparent from 2 to 4 weeks after birth, but not before or after these ages (Figure 1B). This observation suggests some compensatory mechanisms for cGKII deficiency. Besides signaling via Runx2, PTH/PTHrP, and the CNP-related factors described above, GSK-3α (the other GSK-3 in mammals) might substitute for GSK-3β, because it was not found to be a phosphorylation target of cGKII (Figure 2D). Although there was no compensatory upregulation in

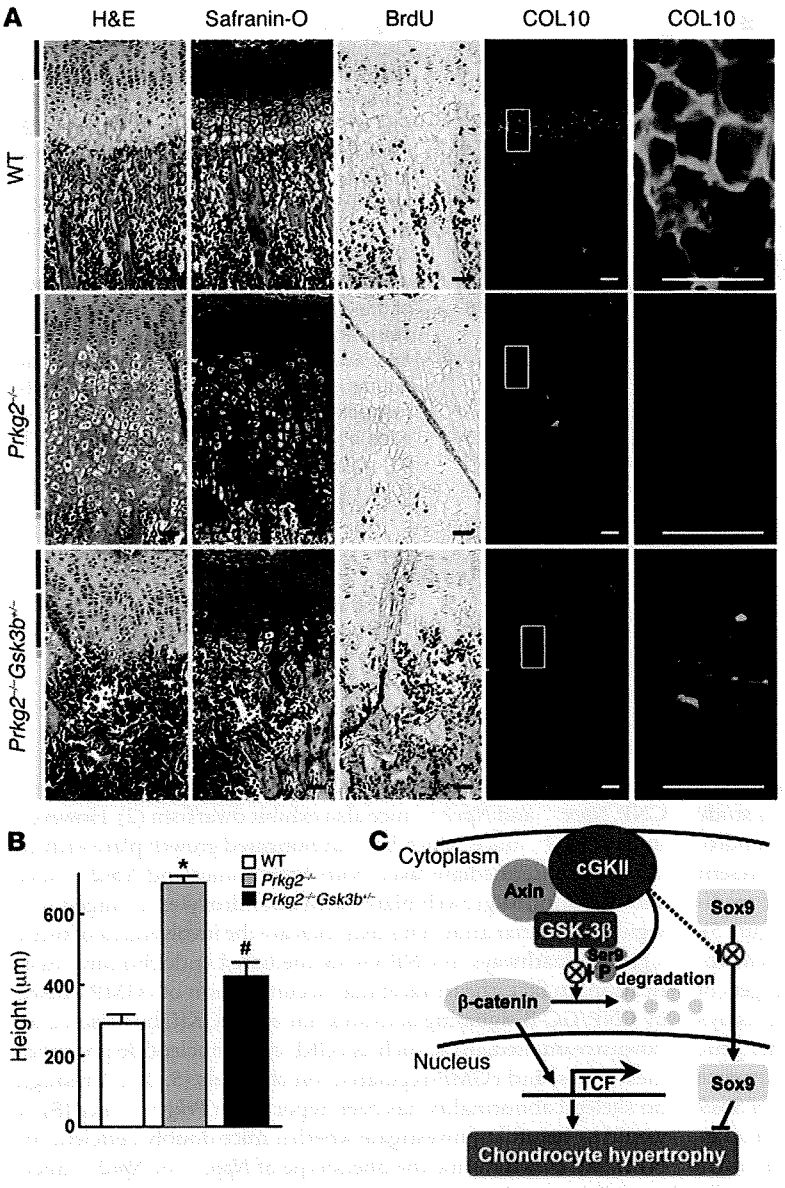

Figure 7
Genetic rescue of growth plate abnormality in *Prkg2*$^{-/-}$ mice by GSK-3β insufficiency. (**A**) H&E staining, Safranin-O staining, BrdU labeling, and immunohistochemical staining of COL10 in the tibial growth plates of 3-week-old mice of the 3 genotypes. Blue, red, green, and yellow bars indicate proliferative zone, abnormal intermediate layer, hypertrophic zone, and primary spongiosa, respectively. Boxed regions in COL10 panels are shown at higher magnification to the right. Scale bars: 50 μm. (**B**) Height of the growth plates of the 3 genotypes. The percentage recovery by the GSK-3β insufficiency was 36.0%. Data are mean ± SD of 4 mice per genotype. $^{*}P < 0.05$ versus WT. $^{\#}P < 0.05$ versus *Prkg2*$^{-/-}$. (**C**) Schematic of the mechanism whereby cGKII promotes growth plate chondrocyte hypertrophy during skeletal growth.

GSK-3 levels in cells lacking either GSK-3α or GSK-3β, functional redundancy of the 2 GSK-3 homologs in β-catenin/TCF–mediated transcription was previously shown using an allelic series of embryonic stem cell lines (17, 30). In fact, *Gsk3b*$^{+/-}$ mice (Supplemental Figure 3) and *Gsk3a*$^{-/-}$ mice (31) showed normal skeletal development and growth. *Gsk3b*$^{-/-}$ mice developed relatively normally until late gestation, when massive liver apoptosis causes embryonic lethality (17); the implication of this finding is that GSK-3α can compensate for GSK-3β deficiency in early stages of mouse development, but cannot substitute for it in all respects. Hence, the age-dependent balance between GSK-3α and GSK-3β might explain the temporary growth plate abnormality in *Prkg2*$^{-/-}$ mice.

GSK-3β is known to be active under resting conditions and inactivated upon stimulation by several signaling pathways, such as Wnt and insulin/Akt; however, the role of phosphorylation of GSK-3β remains controversial (32, 33). Our present results led us to propose cGKII as a novel regulator of GSK-3β and showed that the β-catenin activity enhanced by cGKII was suppressed by GSK-3β^{S9A}, indicating the mediation of GSK-3β phosphorylation at Ser9 in cGKII/β-catenin signaling (Figure 4C). Conversely, several reports showed that GSK-3β inactivation causing β-catenin induction by Wnt stimulation depends not on Ser9 phosphorylation, but rather on coupling with the scaffolding protein, such as Axin (34, 35). The present study, however, showed that cGKII formed a complex with Axin and further phosphorylated GSK-3β that bound to Axin (Figure 4D), suggesting some interaction between Ser9 phosphorylation and coupling with Axin in the regulation of GSK-3β by cGKII. In fact, a previous report proposed that Wnt signaling, similar to insulin/Akt signaling, induces GSK-3β phosphorylation via the interaction between the signaling pathways both in neuronal PC12 cells and in human embryonic kidney 293T cells (36). While these findings imply a possible link between cGKII/β-catenin and canonical Wnt/β-catenin signaling, we note that there is no direct evidence of cGKII being involved in the canonical Wnt pathway. We therefore believe that cGKII/β-catenin signaling, which is dependent on GSK-3β phosphorylation, may have a mechanism that is, at least in part, distinct from that of Wnt/β-catenin signaling. Further studies will be needed to clarify the details of GSK-3β–related signaling not only in chondrocytes, but also in other cells.

We conclude that cGKII promotes chondrocyte hypertrophy and skeletal growth through phosphorylation and inactivation of GSK-3β. For the application of this intracellular signaling to yield novel therapeutics for skeletal disorders, we are now developing a gene transfer system using biocompatible polyplex nanomicelles (37, 38). Further understanding of the molecular signaling related to the cGKII/GSK-3β axis, in combination with other putative signaling systems, will greatly assist in unraveling the molecular network that modulates endochondral ossification and skeletal growth.

Methods

Animals. The *Prkg2*$^{-/-}$ mice and *Gsk3b*$^{+/-}$ mice were maintained in a C57BL/6 background. To generate *Prkg2*$^{-/-}$*Gsk3b*$^{+/-}$ mice, *Gsk3b*$^{+/-}$ mice were mated with the homozygous *Prkg2*$^{-/-}$ mice to obtain *Prkg2*$^{+/-}$*Gsk3b*$^{+/-}$ mice, which were then mated with each other. All experiments were performed on male mice and were approved by the Animal Care and Use Committee of the University of Tokyo.

Radiological and histological analyses. Plain radiographs were taken using a soft X-ray apparatus (Softex CMB-2; Softex). For histological analyses, skeletons were fixed in 4% paraformaldehyde, decalcified with 10% EDTA, embedded in paraffin, sectioned in 5-μm slices, and stained with H&E or Safranin-O, according to standard procedures. For BrdU labeling, mice were injected intraperitoneally with BrdU (25 μg/g body weight) 2 h prior to sacrifice, and the sections were stained with a BrdU staining kit (Zymed Laboratories) according to the manufacturer's instructions. In situ hybridization with nonradioactive probes was performed as previously described (39). For immunohistochemistry, antibodies to cGKII, Ser9-phosphorylated GSK-3β, MMP-13, Runx2 (1:50; Santa Cruz Biotechnology Inc.), GSK-3β (1:200; Chemicon), COL10 (1:1000; LSL), β-catenin (1:100; Cell Signaling Technology), and respective nonimmune serums were used, and the signal was detected with an HRP-conjugated secondary antibody. For fluorescent visualization, a secondary antibody conjugated with Alexa Fluor 488 (Invitrogen) was used.

Cell cultures. ATDC5 cells were grown and maintained in DMEM and F12 at a 1:1 ratio with 5% FBS. To induce hypertrophic differentiation, the ATDC5 cells were cultured in the presence of insulin, transferrin and sodium selenite (ITS) supplement (Sigma-Aldrich) for 21 d as described previously (40). We confirmed COL10 expression by real-time RT-PCR and used the cells whose stage of differentiation was assumed to be prehypertrophic or hypertrophic. Primary chondrocytes were isolated by digestion of E18.5 costal cartilage. Primary chondrocytes, HuH-7 cells, HEK293 cells, and HeLa cells were cultured in high-glucose DMEM with 10% FBS. Three-dimensional alginate bead cultures of primary costal chondrocytes and ATDC5 cells were performed with or without LiCl (8 mM) for 72 h, and the cells were analyzed as described previously (21). For immunocytochemistry of primary costal chondrocytes, the cell colonies were fixed with 4% paraformaldehyde, embedded in paraffin, sectioned in 5-μm slices, and underwent immunostaining for COL10 and MMP-13 as described above. For ALP staining, sections were fixed in 70% ethanol and stained for 10 min with a solution containing 0.01% Naphthol AS-MX phosphate disodium salt (Sigma-Aldrich), 1% N, N-dimethyl-formamide (Wako Pure Chemical Industries Ltd.), and 0.06% fast blue BB (Sigma-Aldrich).

In vitro kinase assay. ATDC5 cells were cultured in the presence of ITS for 21 d to differentiate into prehypertrophic or hypertrophic chondrocytes, as described above. The whole-cell lysate of the differentiated cells was prepared using Cell Lysis Buffer (Cell Signaling Technology). The cell lysate or recombinant GSK-3β (Upstate Biotechnology Inc.) was incubated with recombinant cGKII (Sigma-Aldrich) in a reaction buffer (Cell Signaling Technology) containing 1.6 mM ATP and 100 μM 8-bromo-cGMP (Biomol) at 30°C for 30 min. An equal amount of protein (15 μg) was subjected to SDS-PAGE and transferred onto nitrocellulose membranes. IB was then performed using primary antibodies to Ser9-phosphorylated GSK-3β (Cell Signaling Technology), GSK-3β (Chemicon), Ser21-phosphorylated GSK-3α and GSK-3α (Cell Signaling Technology), and β-actin (Sigma-Aldrich). The membrane was incubated with HRP-conjugated antibody (Promega), and the immunoreactive proteins were visualized with ECL Plus (Amersham Biosciences).

Plasmids and viral vectors. cDNA of caspase-9 (GenBank accession no. NM_001229.1), Bad (NM_007522.2), PLK (NM_011121.3), p90RSK (NM_009097.4), eNOS (NM_000603.3), GSK-3β (NM_002093.2), VASP (NM_009499.1), cdc25 (NM_009860.2), and cysteine- and glycine-rich protein 2 (CSRP2; NM_007792.3) was ligated into pCMV-HA (Invitrogen). cDNA of rat cGKII (NM_013012.1; nucleotides 48–2,333) was ligated into pcDNA4HisA (Invitrogen). A PCR-amplified fragment (nucleotides 48–1,403) was used to construct the cGKII-Δkinase plasmid. Plasmids encoding constitutively active human cGKII were kindly provided by B.M. Hogema (Erasmus University Medical Center, Rotterdam, The Netherlands; ref. 41). Axin1 (NM_003502.2) was subcloned into pCMV-Myc (Invitrogen) to introduce Myc epitope tags. cDNA of Sox9 (NM_000346.2) and Runx2 (NM_009820.3) was ligated into pEGFPC1 (Clontech) to generate GFP-tagged plasmids. To create phosphorylation-deficient mutants, GFP-tagged Sox9 plasmid and GSK-3β plasmid were subjected to site-directed mutagenesis using the inverse PCR technique. All constructs were verified by sequencing. cGKII, cGKII-Δkinase, GSK-3β^{S9A}, and control GFP retrovirus vectors were constructed using pMx vector and plat-E cells as described previously (42).

Gene transfection. For the transient transfection, a total of 1 μg plasmid DNA was transfected using Fugene6 (Roche). For cotransfection, all plasmids were added in an equal ratio. Total RNA was isolated 72 h after the transfection and used for the subsequent assays. For fluorescent detection, HeLa cells were transiently transfected, and fluorescent images were taken 24 h after transfection. To investigate the interaction of cGKII and MAPK/STAT signaling, ATDC5 cells were transfected with cGKII or the empty vector, and FGF-2 (1 ng/ml) was added 72 h after transfection. IB was then carried out using primary antibodies to p-Erk1/2, Erk1/2, p-p38MAPK, p38MAPK, p-JNK2/3, JNK2/3, p-JNK1, JNK1, p-STAT1, and STAT1 (Cell Signaling Technology) as described above.

Real-time RT-PCR. Total RNA was reverse-transcribed with MultiScribe RT (Applied Biosystems Inc.). Semiquantitative RT-PCR was performed within an exponential phase of the amplification, with the following primer sequences: caspase-9 forward, 5′-CGATGCAGGGTGCGCCTAGTGA-3′; caspase-9 reverse, 5′-TGACCAGCTGCCTGGCCTGATC-3′; Bad forward, 5′-CCAGGTCTCCTGGGGAGCAACATTC-3′; Bad reverse, 5′-AGCTCCTCCTCCATCCCTTCATCC-3′; PLK forward, 5′-TGGCACTCCTAACTACATAGCTCCTGAGG-3′; PLK reverse, 5′-CGGAGGTAGGTCTCTTTTAGGCACGA-3′; p90RSK forward, 5′-GATTCTTCTGCGGTATGGCCA-3′; p90RSK reverse, 5′-TGCCGTAGGATCTTATCCAGCA-3′; eNOS forward, 5′-CTCGAGTGGTTTGCTGCCCTTG-3′; eNOS reverse, 5′-CAGGTCCCTCATGCCAATCTCTGA-3′; GSK-3β forward, 5′-CCAGTATAGATGTATGGTCTG-3′; GSK-3β reverse, 5′-CTTGTTGGTGTTCCTAGG-3′; VASP forward, 5′-TTCCAGCCGGGCTACTGTGATG-3′; VASP reverse, 5′-CGGCCAACAACTCGGAAGGAGT-3′; cdc25 forward, 5′-GCACTGGAAAGGGTGGAGAGACTGG-3′; cdc25 reverse, 5′-CCTCTTCACTTGCAGGTGGGATAGG-3′; Runx2 forward, 5′-CCCAGCCACCTTTACCTACA-3′; Runx2 reverse, 5′-TATGGAGTGCTGCTGGTCTG-3′. Real-time RT-PCR was performed on an ABI 7700 Sequence Detection system (Applied Biosystems) using QuantiTect SYBR Green PCR Master Mix (Qiagen) with β-actin as the internal control and the following primer sequences: COL10 forward, 5′-CATAAAGGGCCCACTTGCTA-3′; COL10 reverse, 5′-TGGCTGATATTCCTGGTGGT-3′; ALP forward, 5′-GCTGATCATTCCCACGTTTT-3′; ALP reverse, 5′-CTGGGCCTGGTAGTTGTTGT-3′; MMP-13 forward, 5′-AGGCCTTCAGAAAAGCCTTC-3′; MMP-13 reverse, 5′-TCCTTGGAGTGATCCAGACC-3′; β-actin forward, 5′-AGATGTGGATCAGCAAGCAG-3′; β-actin reverse, 5′-GCGCAAGTTAGGTTTTGTCA-3′. All reactions were run in triplicate.

Luciferase reporter gene assay. The human COL10 promoter regions from −4,459 bp relative to the transcriptional start site were cloned into the pGL3-Basic vector (Promega). The TOPflash system (Upstate Biotechnology Inc.) was used according to the manufacturer's protocol. The luciferase assay was performed with a dual-luciferase reporter assay system (Promega) using a GloMax 96 Microplate Luminometer (Promega).

IP and IB assay. IP was performed with ProFound Myc Tag IP/Co-IP kits (Pierce) according to the manufacturer's protocol. Samples were prepared using M-PER or NE-PER (Pierce) supplemented with 2 mM Na_3VO_4 and 10 mM NaF according to the manufacturer's protocol. Cell lysates were incubated with the high-affinity anti-c-Myc antibody-coupled agarose

at 4°C overnight. Immunocomplexes were washed 3 times with cold wash solution. c-Myc–tagged proteins were eluted, and an equal amount of each eluted sample (15 μg) was subjected to SDS-PAGE, transferred onto nitrocellulose membranes, and subjected to IB using primary antibodies to cGKII (Santa Cruz Biotechnology Inc.), GSK-3β and Ser9-phosphorylated GSK-3β (Chemicon), and Myc tag (Upstate Biotechnology Inc.). Immunoreactive proteins were visualized as described above.

Statistics. Means of groups were compared by ANOVA, and significance of differences was determined by post-hoc testing by the Bonferroni method. A P value less than 0.05 was considered significant.

Acknowledgments

We thank Boris M. Hogema for providing plasmids encoding constitutively active human cGKII; Henry Kronenberg and Sakae Tanaka for critical discussions; and Reiko Yamaguchi and Mizue Ikeuchi for their excellent technical help. This work was supported by Grant-in-Aid no. 14657359 for Scientific Research from the Japanese Ministry of Education, Culture, Sports, Science and Technology.

Received for publication February 5, 2008, and accepted in revised form May 7, 2008.

Address correspondence to: Hiroshi Kawaguchi, Sensory and Motor System Medicine, Faculty of Medicine, University of Tokyo, Hongo 7-3-1, Bunkyo-ku, Tokyo 113-8655, Japan. Phone: 81-33815-5411 ext. 30473; Fax: 81-33818-4082; E-mail: kawaguchi-ort@h.u-tokyo.ac.jp.

1. Kronenberg, H.M. 2003. Developmental regulation of the growth plate. *Nature.* **423**:332–336.
2. Chusho, H., et al. 2001. Dwarfism and early death in mice lacking C-type natriuretic peptide. *Proc. Natl. Acad. Sci. U. S. A.* **98**:4016–4021.
3. Tamura, N., et al. 2004. Critical roles of the guanylyl cyclase B receptor in endochondral ossification and development of female reproductive organs. *Proc. Natl. Acad. Sci. U. S. A.* **101**:17300–17305.
4. Bartels, C.F., et al. 2004. Mutations in the transmembrane natriuretic peptide receptor NPR-B impair skeletal growth and cause acromesomelic dysplasia, type Maroteaux. *Am. J. Hum. Genet.* **75**:27–34.
5. Schulz, S. 2005. C-type natriuretic peptide and guanylyl cyclase B receptor. *Peptides.* **26**:1024–1034.
6. Pfeifer, A., et al. 1996. Intestinal secretory defects and dwarfism in mice lacking cGMP-dependent protein kinase II. *Science.* **274**:2082–2086.
7. Pfeifer, A., et al. 1999. Structure and function of cGMP-dependent protein kinases. *Rev. Physiol. Biochem. Pharmacol.* **135**:105–149.
8. Pfeifer, A., et al. 1998. Defective smooth muscle regulation in cGMP kinase I-deficient mice. *EMBO J.* **17**:3045–3051.
9. Chikuda, H., et al. 2004. Cyclic GMP-dependent protein kinase II is a molecular switch from proliferation to hypertrophic differentiation of chondrocytes. *Genes Dev.* **18**:2418–2429.
10. Doble, B.W., and Woodgett, J.R. 2003. GSK-3: tricks of the trade for a multi-tasking kinase. *J. Cell Sci.* **116**:1175–1186.
11. Holmbeck, K. 2005. Collagenase in cranial morphogenesis. *Cells Tissues Organs.* **181**:154–165.
12. Akiyama, H., Chaboissier, M.C., Martin, J.F., Schedl, A., and de Crombrugghe, B. 2002. The transcription factor Sox9 has essential roles in successive steps of the chondrocyte differentiation pathway and is required for expression of Sox5 and Sox6. *Genes Dev.* **16**:2813–2828.
13. Takeda, S., Bonnamy, J.P., Owen, M.J., Ducy, P., and Karsenty, G. 2001. Continuous expression of Cbfa1 in nonhypertrophic chondrocytes uncovers its ability to induce hypertrophic chondrocyte differentiation and partially rescues Cbfa1-deficient mice. *Genes Dev.* **15**:467–481.
14. Ornitz, D.M. 2005. FGF signaling in the developing endochondral skeleton. *Cytokine Growth Factor Rev.* **16**:205–213.
15. Yasoda, A., et al. 2004. Overexpression of CNP in chondrocytes rescues achondroplasia through a MAPK-dependent pathway. *Nat. Med.* **10**:80–86.
16. Deng, C., Wynshaw-Boris, A., Zhou, F., Kuo, A., and Leder, P. 1996. Fibroblast growth factor receptor 3 is a negative regulator of bone growth. *Cell.* **84**:911–921.
17. Hoeflich, K.P., et al. 2000. Requirement for glycogen synthase kinase-3beta in cell survival and NF-kappaB activation. *Nature.* **406**:86–90.
18. Huang, L.F., Fukai, N., Selby, P.B., Olsen, B.R., and Mundlos, S. 1997. Mouse clavicular development: analysis of wild-type and cleidocranial dysplasia mutant mice. *Dev. Dyn.* **210**:33–40.
19. Dong, Y.F., Soung do, Y., Schwarz, E.M., O'Keefe, R.J., and Drissi, H. 2006. Wnt induction of chondrocyte hypertrophy through the Runx2 transcription factor. *J. Cell Physiol.* **208**:77–86.
20. Hartmann, C., and Tabin, C.J. 2000. Dual roles of Wnt signaling during chondrogenesis in the chicken limb. *Development.* **127**:3141–3159.
21. Yano, F., et al. 2005. The canonical Wnt signaling pathway promotes chondrocyte differentiation in a Sox9-dependent manner. *Biochem. Biophys. Res. Commun.* **333**:1300–1308.
22. Tamamura, Y., et al. 2005. Developmental regulation of Wnt/beta-catenin signals is required for growth plate assembly, cartilage integrity, and endochondral ossification. *J. Biol. Chem.* **280**:19185–19195.
23. Akiyama, H., et al. 2004. Interactions between Sox9 and beta-catenin control chondrocyte differentiation. *Genes Dev.* **18**:1072–1087.
24. Schlossmann, J., and Hofmann, F. 2005. cGMP-dependent protein kinases in drug discovery. *Drug Discov. Today.* **10**:627–634.
25. Hunziker, E.B. 1994. Mechanism of longitudinal bone growth and its regulation by growth plate chondrocytes. *Microsc. Res. Tech.* **28**:505–519.
26. Wilsman, N.J., Farnum, C.E., Leiferman, E.M., Fry, M., and Barreto, C. 1996. Differential growth by growth plates as a function of multiple parameters of chondrocytic kinetics. *J. Orthop. Res.* **14**:927–936.
27. Kronenberg, H.M. 2006. PTHrP and skeletal development. *Ann. N. Y. Acad. Sci.* **1068**:1–13.
28. Pilz, R.B., and Casteel, D.E. 2003. Regulation of gene expression by cyclic GMP. *Circ. Res.* **93**:1034–1046.
29. Miyazawa, T., et al. 2002. Cyclic GMP-dependent protein kinase II plays a critical role in C-type natriuretic peptide-mediated endochondral ossification. *Endocrinology.* **143**:3604–3610.
30. Doble, B.W., Patel, S., Wood, G.A., Kockeritz, L.K., and Woodgett, J.R. 2007. Functional redundancy of GSK-3alpha and GSK-3beta in Wnt/beta-catenin signaling shown by using an allelic series of embryonic stem cell lines. *Dev. Cell.* **12**:957–971.
31. MacAulay, K., et al. 2007. Glycogen synthase kinase 3alpha-specific regulation of murine hepatic glycogen metabolism. *Cell Metab.* **6**:329–337.
32. Patel, S., Doble, B., and Woodgett, J.R. 2004. Glycogen synthase kinase-3 in insulin and Wnt signalling: a double-edged sword? *Biochem. Soc. Trans.* **32**:803–808.
33. Dominguez, I., and Green, J.B. 2001. Missing links in GSK3 regulation. *Dev. Biol.* **235**:303–313.
34. Papadopoulou, D., Bianchi, M.W., and Bourouis, M. 2004. Functional studies of shaggy/glycogen synthase kinase 3 phosphorylation sites in Drosophila melanogaster. *Mol. Cell. Biol.* **24**:4909–4919.
35. Ding, V.W., Chen, R.H., and McCormick, F. 2000. Differential regulation of glycogen synthase kinase 3beta by insulin and Wnt signaling. *J. Biol. Chem.* **275**:32475–32481.
36. Fukumoto, S., et al. 2001. Akt participation in the Wnt signaling pathway through Dishevelled. *J. Biol. Chem.* **276**:17479–17483.
37. Itaka, K., et al. 2007. Bone regeneration by regulated in vivo gene transfer using biocompatible polyplex nanomicelles. *Mol. Ther.* **15**:1655–1662.
38. Ohba, S., et al. 2007. Identification of a potent combination of osteogenic genes for bone regeneration using embryonic stem (ES) cell-based sensor. *FASEB J.* **21**:1777–1787.
39. Kamekura, S., et al. 2006. Contribution of runt-related transcription factor 2 to the pathogenesis of osteoarthritis in mice after induction of knee joint instability. *Arthritis Rheum.* **54**:2462–2470.
40. Shukunami, C., et al. 1997. Cellular hypertrophy and calcification of embryonal carcinoma-derived chondrogenic cell line ATDC5 in vitro. *J. Bone Miner. Res.* **12**:1174–1188.
41. Vaandrager, A.B., et al. 2003. Autophosphorylation of cGMP-dependent protein kinase type II. *J. Biol. Chem.* **278**:28651–28658.
42. Saito, T., Ikeda, T., Nakamura, K., Chung, U.I., and Kawaguchi, H. 2007. S100A1 and S100B, transcriptional targets of SOX trio, inhibit terminal differentiation of chondrocytes. *EMBO Rep.* **8**:504–509.

ARTHRITIS & RHEUMATISM
Vol. 58, No. 9, September 2008, pp 2764–2775
DOI 10.1002/art.23805

The Distinct Role of the Runx Proteins in Chondrocyte Differentiation and Intervertebral Disc Degeneration

Findings in Murine Models and in Human Disease

Shingo Sato,[1] Ayako Kimura,[1] Jerfi Ozdemir,[2] Yoshinori Asou,[1] Makiko Miyazaki,[1] Tetsuya Jinno,[1] Keisuke Ae,[1] Xiuyun Liu,[2] Mitsuhiko Osaki,[3] Yasuhiro Takeuchi,[4] Seiji Fukumoto,[5] Hiroshi Kawaguchi,[5] Hirotaka Haro,[6] Ken-ichi Shinomiya,[1] Gerard Karsenty,[2] and Shu Takeda[1]

Objective. **Runx2 is a transcription factor that regulates chondrocyte differentiation. This study was undertaken to address the role of the different Runx proteins (Runx1, Runx2, or Runx3) in chondrocyte differentiation using chondrocyte-specific *Runx*–transgenic mice, and to study the importance of the QA domain of Runx2, which is involved in its transcriptional activation.**

Methods. ***Runx*** **expression was analyzed in the mouse embryo by in situ hybridization. Overexpression of *Runx*1, *Runx*2 (lacking the QA domain [ΔQA]), or *Runx*3 was induced in chondrocytes in vivo, to produce α(1)II-*Runx*1, α(1)II-*Runx*2ΔQA, and α(1)II-*Runx*3 mice, respectively, for histologic and molecular analyses. Runx expression was also examined in an experimental mouse model of mechanical stress–induced intervertebral disc (IVD) degeneration and in human patients with IVD degeneration.**

Results. ***Runx*1 expression was transiently observed in condensations of mesenchymal cells, whereas *Runx*2 and *Runx*3 were robustly expressed in prehypertrophic chondrocytes. Similar to α(1)II-*Runx*2 mice, α(1)II-*Runx*2ΔQA and α(1)II-*Runx*3 mice developed ectopic mineralization of cartilage, but this was less severe in the α(1)II-*Runx*2ΔQA mice. In contrast, α(1)II-*Runx*1 mice displayed no signs of ectopic mineralization. Surprisingly, α(1)II-*Runx*1 and α(1)II-*Runx*2 mice developed scoliosis due to IVD degeneration, characterized by an accumulation of extracellular matrix and ectopic chondrocyte hypertrophy. During mouse embryogenesis, Runx2, but not Runx1 or Runx3, was expressed in the IVDs. Moreover, both in the mouse model of IVD degeneration and in human patients with IVD degeneration, there was significant up-regulation of Runx2 expression.**

Conclusion. **Each Runx protein has a distinct, yet overlapping, role during chondrocyte differentiation. Runx2 contributes to the pathogenesis of IVD degeneration.**

Cells of the chondrocyte lineage play critical roles at several stages of endochondral ossification (1). Chondrocytes are the first skeletal-specific cell type that can be identified in the condensations of mesenchymal cells that precede the development of skeletal elements (2).

Supported by Grant-in-Aid for Scientific Research grants from the Japan Society for the Promotion of Science to Drs. Asou, Jinno, Ae, Shinomiya, and Takeda, and by 21st Century Center of Excellence Program grants from the Ministry of Education, Culture, Sports, Science, and Technology of Japan to Drs. Shinomiya and Takeda. Dr. Takeda's work also was supported by grants from Uehara Memorial Foundation. Dr. Karsenty's work was supported by a grant from the NIH.

[1]Shingo Sato, MD, PhD, Ayako Kimura, MS, Yoshinori Asou, MD, PhD, Makiko Miyazaki, MD, Tetsuya Jinno, MD, PhD, Keisuke Ae, MD, PhD, Ken-ichi Shinomiya, MD, PhD, Shu Takeda, MD, PhD: Tokyo Medical and Dental University, Tokyo, Japan; [2]Jerfi Ozdemir, BSc, MBA, Xiuyun Liu, Gerard Karsenty, MD, PhD (current address: Columbia University, New York, New York): Baylor College of Medicine, Houston, Texas; [3]Mitsuhiko Osaki, PhD: Tottori University, Tottori, Japan; [4]Yasuhiro Takeuchi, MD, PhD: Toranomon Hospital, Tokyo, Japan; [5]Seiji Fukumoto, MD, PhD, Hiroshi Kawaguchi, MD, PhD: University of Tokyo, Tokyo, Japan; [6]Hirotaka Haro, MD, PhD: University of Yamanashi, Yamanashi, Japan.

Dr. Sato, Ms Kimura, and Ms Ozdemir contributed equally to this work.

Dr. Takeuchi has received speaking fees from Eisai Company, Ltd. and Teijin Pharma, Ltd. (less than $10,000 each).

Address correspondence and reprint requests to Shu Takeda, MD, PhD, Department of Orthopedic Surgery, Tokyo Medical and Dental University, 1-5-45 Yushima, Bunkyo-ku, Tokyo 113-8519, Japan. E-mail: shu-tky@umin.ac.jp.

Submitted for publication February 14, 2008; accepted in revised form May 29, 2008.

At these initial stages of development, chondrocytes actively divide or proliferate, and express a specific molecular marker, α1(II) collagen. Around embryonic day 14.5 of mouse development, chondrocytes in the center of these mesenchymal condensations become hypertrophic and form 2 distinct cell populations: prehypertrophic chondrocytes that continue to express α1(II) collagen, and hypertrophic chondrocytes that exit the cell cycle and express α1(X) collagen as a specific molecular marker (3). Hypertrophic chondrocytes replace the extracellular matrix with one that is permissive to vascular invasion; this allows the entry of osteoblastic cells. Subsequently, and at either end of a given skeletal element, chondrocytes organize into columns, forming growth-plate cartilage, which is responsible for linear skeletal growth (1).

Major progress has been made, over the last decade, in our understanding of the transcriptional control of chondrocyte differentiation (2). Work in multiple laboratories has established the critical role of Sox9 (4), along with Sox5 and Sox6 (5), in the differentiation of nonhypertrophic chondrocytes. Meanwhile, Runx2 (6–8), together with Runx3 (9), has been shown to favor chondrocyte hypertrophy. We previously demonstrated that continuous expression of *Runx*2 in nonhypertrophic chondrocytes (herein comprising the α(1)II-*Runx*2 group of mice) led to the development of ectopic hypertrophy of chondrocytes, followed by bone formation (7).

Runx1, the other member of the Runx family, shares a highly homologous DNA binding domain, the runt domain, with Runx2 and Runx3. There are also homologous regions N-terminal to the runt domain that are common to Runx1, Runx2, and Runx3. Although the last 5 amino acids of all 3 Runx proteins are identical, Runx2 possesses a unique QA domain composed of a stretch of Q and A residues (10).

Currently, it is unknown whether a functional hierarchy exists among Runx2, Runx3, and Runx1 (10). In addition, the significance of the QA domain of Runx2 in inducing chondrocyte differentiation remains to be elucidated. Therefore, in the present study, we generated transgenic mice that overexpressed *Runx*1 or *Runx*3 or lacked a QA domain in *Runx*2 (comprising the α(1)II-*Runx*1, α(1)II-*Runx*3, and α(1)II-*Runx*2ΔQA groups of mice, respectively). The mice were generated using the identical promoter/enhancer construct that we have previously used to specifically express *Runx*2 in chondrocytes (7).

Our results showed that all 3 *Runx* genes were expressed in cells of the chondrocyte lineage, but each functioned differently in these cells. The α(1)II-*Runx*3 and α(1)II-*Runx*2ΔQA mice developed ectopic differentiation of hypertrophic chondrocytes in chondrocostal cartilage, albeit to a lesser extent in the α(1)II-*Runx*2ΔQA mice. Surprisingly, α(1)II-*Runx*1 and α(1)II-*Runx*2 mice exhibited a kyphotic deformity of the vertebrae due to intervertebral disc (IVD) degeneration. We therefore studied an experimental mouse model of mechanical stress–induced IVD degeneration, which showed that Runx2, but not Runx1 or Runx3, was induced in the degenerated IVD. In addition, in human patients with IVD degeneration, we found that Runx2 expression was up-regulated, thus substantiating the pathophysiologic importance of Runx2 in the development of IVD degeneration in humans. This study illustrates the specific and distinct role of the *Runx* genes in physiologic conditions such as chondrocytic differentiation, and in pathologic conditions such as IVD degeneration.

MATERIALS AND METHODS

Generation of transgenic mice and analysis of transgene expression. The α1(II)-*Runx*1, α1(II)-*Runx*3, and α1(II)-*Runx*2ΔQA transgenes were obtained by subcloning *Runx*1, *Runx*3, or *Runx*2ΔQA complementary DNA (cDNA) (11) into an α1(II) collagen–expressing chondrocyte–specific promoter cassette (7). Transgenic founders were obtained by pronuclear injection into C57BL/6 oocytes, as previously described (7). We thus obtained multiple lines of transgenic mice with identical phenotypes in all groups except for the α1(II)-*Runx*3 mice. The *Runx*2-deficient mice were a generous gift from Dr. M. Owen (12). Wild-type (WT) mice were purchased from Jackson Laboratories (Bar Harbor, ME).

The genotypes of the mice were determined by polymerase chain reaction (PCR). (A list of the PCR primer sequences is available upon request from the corresponding author.) Chondrocyte RNA was extracted from chondrocostal cartilage of the transgenic mouse embryos, using TRIzol (Invitrogen, Carlsbad, CA), and was then reverse-transcribed for cDNA synthesis. Expression of the transgene was analyzed quantitatively by real-time quantitative PCR (MX3000P; Stratagene, La Jolla, CA). Primers were designed against the specific poly(A) region of the transgene, which is common to all 3 transgenes, namely 5′-GCGTGCATGCGACGTCATAGCTCTC-3′ (forward) and 5′-GGTTCAGGGGGAGGTGTGGGAGG-3′ (reverse). Four mice per group were analyzed.

Skeletal preparations. To prepare skeletal specimens for analysis, groups of mouse skeletons were dissected at each indicated time point of development and skinned. Subsequently, the skeletons were fixed in 100% ethanol at 4°C overnight, and stained with Alcian blue dye for 1 day followed by staining with alizarin red solution according to the standard protocol (7). Specimens were cleared in 50% glycerol/50% ethanol until soft tissue staining was removed. Six mice per group were analyzed, and identical phenotypes were observed.

Histology, in situ hybridization, and immunohistochemistry. For histologic examination, tissue samples from the embryos were immediately fixed in 4% paraformaldehyde/phosphate buffered saline after dissection, dehydrated with gradually increasing concentrations of ethanol, and embedded

in paraffin. Tissue samples from adult mice were decalcified in 20% EDTA for 2 weeks after fixation before being embedded in paraffin. Sections were stained with 0.1% Safranin O (orange stain) to evaluate cartilage matrices, and 0.03% fast green to evaluate morphologic features, as previously described (13). In situ hybridization was performed using ^{35}S-labeled riboprobes according to the standard protocol as described previously (7). Hybridizations were performed at 55°C.

Autoradiography and Hoechst 33528 staining were performed as previously described (7). For staining with LacZ, tails from Runx2-heterozygote mice were fixed in 0.2% paraformaldehyde at room temperature for 30 minutes, and then stained overnight in X-Gal solution as previously described (7). The following day, samples were decalcified and processed for histologic examination.

Immunohistochemistry was performed according to a standard protocol (7). Anti-Runx1 antibody (14) and anti–α1(X) collagen antibody were purchased from Santa Cruz Biotechnology (Santa Cruz, CA) and Cosmo Bio (Tokyo, Japan), respectively. The anti-Runx2 and anti-Runx3 antibodies have been described previously (7,15). Six mice per group were analyzed, and identical phenotypes were observed.

Disc compression of mouse vertebrae and analysis of IVDs in human patients. The vertebrae of 8-week-old female WT mice were compressed as previously described, with minor modifications (16). Briefly, the ninth and tenth caudal vertebrae were percutaneously punctured by 0.4-mm stainless steel pins and transfixed. Subsequently, the pins were instrumented using elastic springs. After 1–4 weeks, the mice were dissected and the vertebrae were examined histologically. Four mice per group were analyzed, and identical phenotypes were observed.

The study protocol involving human patients was approved by a local ethics committee. Patients with IVD degeneration were classified according to an established grading system (17). Patients with moderate disc degeneration (grade 3 to grade 4) (17) gave written informed consent for the collection of their RNA from the degenerated disc at the time of surgery. As a control, we used patients with spinal cord injury whose IVDs had no detectable damage. RNA was extracted from the IVD samples and reverse-transcribed. Expression of *Runx*2 was quantitatively analyzed by real-time quantitative PCR.

RESULTS

Comparison of *Runx*1, *Runx*2, and *Runx*3 expression during mouse skeletal development. As an initial way to assess the respective contribution of each of the 3 *Runx* genes to chondrocyte differentiation, we used in situ hybridization to study their pattern of expression in the developing mouse skeletons between embryonic day 12.5 and birth. The identity of the cells expressing each *Runx* gene was determined on adjacent tissue sections using different probes, as follows: α1(I) collagen as a marker of fibroblasts and osteoblasts, α1(II) collagen as a marker of proliferating and prehypertrophic chondrocytes, α1(X) collagen as a marker of hypertrophic chondrocytes, and Indian hedgehog as a marker of prehypertrophic chondrocytes (18). This analysis was performed in vertebrae and in long bones, since chondrocyte differentiation has been extensively studied on a molecular level in both of these sites.

At embryonic day 12.5, *Runx*2 was expressed in mesenchymal cells of the perichondrium of the vertebrae (Figure 1A, arrow), but not in cells located in the vertebral body. Expression of *Runx*2 was also observed in cells of Meckel's cartilage (results not shown). These results indicate that at this stage of development, *Runx*2 was expressed in prechondrogenic cells. *Runx*1, at embryonic day 12.5, was expressed in α1(II) collagen–positive cells of the perichondrium of the vertebrae (Figure 1A, arrow), as well as in the dorsal root ganglia. In contrast, *Runx*3 expression was observed in chondrocytes in vertebral bodies (Figure 1A, arrowhead).

The chondrocytes of vertebral bodies strongly expressed Indian hedgehog (Figure 1A), suggesting that these chondrocytes were destined to become prehypertrophic. At embryonic day 14.5 and at later stages of embryonic development, *Runx*1 expression in chondrocytes was low, whereas *Runx*2 was expressed in the prehypertrophic and hypertrophic chondrocytes, and *Runx*3 was expressed in the prehypertrophic chondrocytes (Figures 1B and C and results not shown).

Results of these analyses demonstrate that all *Runx* genes are expressed at some developmental point in cells of the chondrocyte lineage. However, they have a complex and dynamic pattern of expression during chondrogenesis. These observations led us to examine the role of each of the Runx proteins in chondrogenesis.

Generation of transgenic mice expressing *Runx*1 or *Runx*3 in nonhypertrophic chondrocytes throughout development. We have previously shown that constitutive expression of *Runx*2 in nonhypertrophic chondrocytes resulted in premature differentiation of hypertrophic chondrocytes in long bones and in ectopic differentiation of hypertrophic chondrocytes in chondrocostal cartilage (7). The high structural similarity of the Runx proteins (Figure 2A) and their overlapping expression in chondrocytes (Figure 1) prompted us to examine the roles of Runx1 and Runx3 in chondrocyte differentiation. To accomplish this, we generated transgenic mice expressing either *Runx*1 or *Runx*3 cDNA under the control of a 3-kb–long fragment of the mouse α1(II) collagen promoter and its 3-kb–long chondrocyte-specific enhancer (19) (Figure 2A); these transgenic mice were termed α1(II)-*Runx*1 and α1(II)-*Runx*3 mice, respectively.

The expression of the transgene in α1(II)-*Runx*1 or α1(II)-*Runx*3 mice was confirmed by real-time quantitative PCR using RNA extracted from transgenic embryos. Transgene expression was restricted to the cartilage, and the expression level was

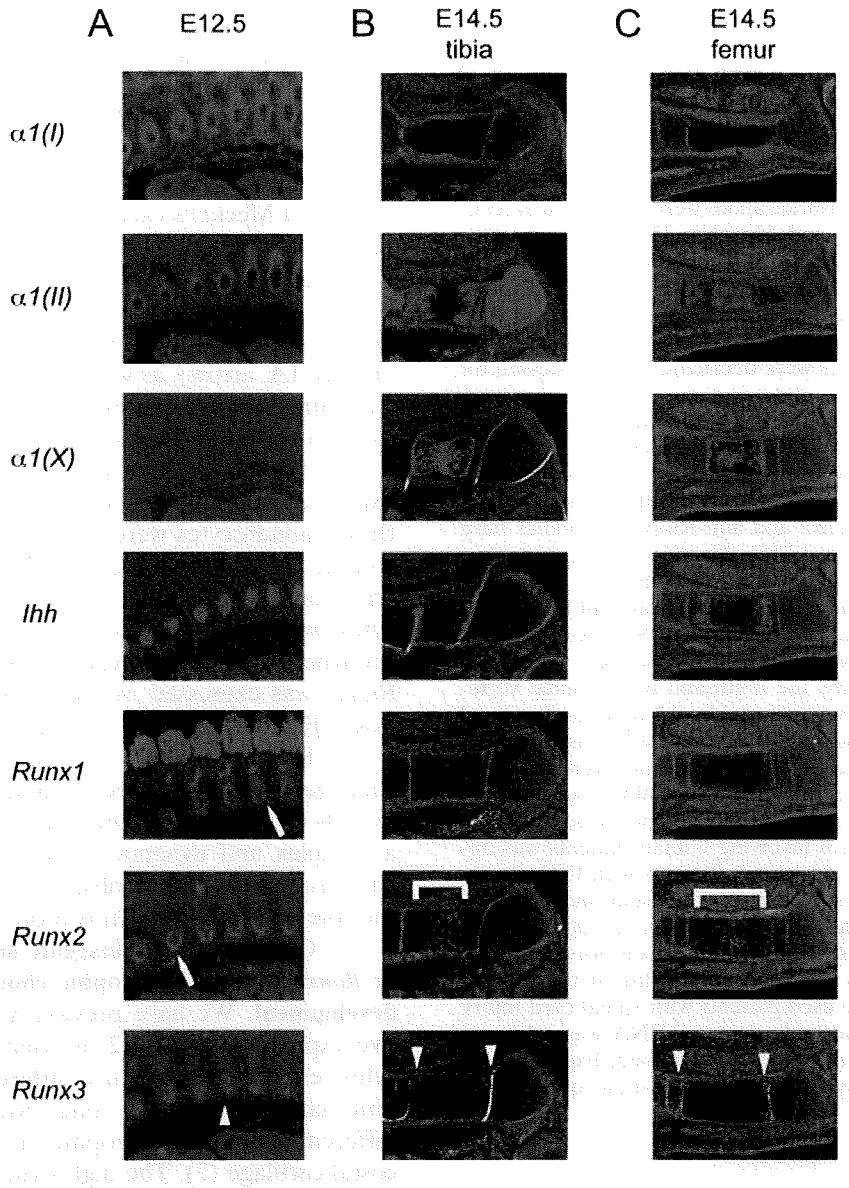

Figure 1. Analysis of *Runx* gene expression by in situ hybridization in the mouse vertebrae at embryonic day (E) 12.5 **(A)** and in the tibia **(B)** and femur **(C)** at embryonic day 14.5. Adjacent sections of wild-type mouse embryos were hybridized with the indicated probes. Note the expression of *Runx*1 and *Runx*2 in condensations of mesenchymal cells **(arrow) (A)**, the broad expression of *Runx*2 in nonhypertrophic chondrocytes **(bracket) (B** and **C)**, and the restricted expression of *Runx*3 in prehypertrophic chondrocytes **(arrowheads) (A–C)**. Ihh = Indian hedgehog.

comparable with that of the α1(II)-*Runx*2 transgene (Figure 2B). We obtained 2 lines for the α1(II)-*Runx*1 mice, and both lines were born at the expected Mendelian ratio and showed no overt abnormalities at birth (results not shown). In contrast, the α1(II)-*Runx*3 mice never survived until birth, and therefore analysis of these mice was performed only on skeletal preparations from transgenic embryos.

Ectopic hypertrophic chondrocyte differentiation and endochondral ossification in α1(II)-*Runx*3 embryos, but not in α1(II)-*Runx*1 mice. In order to study skeletal cell differentiation, we first used Alcian blue/alizarin red to stain skeletal preparations (20). Alcian blue stains were used to reveal demineralization of cartilaginous matrices, while alizarin red stains showed mineralization of cartilaginous and bony matrices.

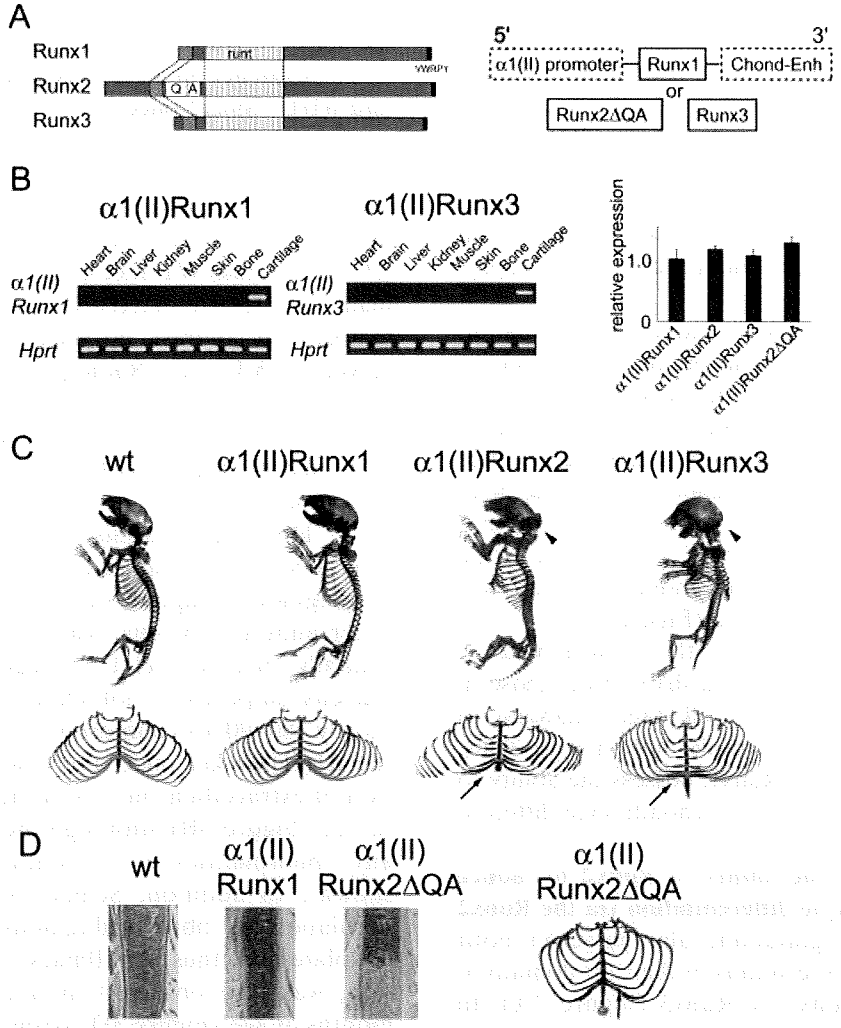

Figure 2. **A** and **B,** Generation of α1(II)-*Runx*–transgenic mice. **A,** Left, Comparison of the structures of the Runx proteins, which share a highly homologous runt domain. Right, Schematic representation of the construct used. Transgenic mice containing *Runx*1, *Runx*2ΔQA (lacking the QA domain of Runx2), or *Runx*3 cDNA were generated under the control of a chondrocyte-specific α1(II) collagen promoter/enhancer (Chond-Enh) cassette. **B,** Left, Cartilage-specific expression of each transgene in the α1(II)-*Runx*1 and α1(II)-*Runx*3 mice. Hypoxanthine guanine phosphoribosyltransferase (*Hprt*) amplification was used as an internal control. Right, Quantitative analysis of transgene expression by real-time polymerase chain reaction. Bars show the mean and SD relative expression. **C** and **D,** Ectopic and accelerated mineralization of cartilage in α1(II)-*Runx* mice as compared with wild-type (WT) mice. **C,** Alcian blue/alizarin red staining of skeletal preparations at birth, revealing ectopically mineralized areas in chondrocostal cartilage (**arrow**) and accelerated chondrocranium mineralization (**arrowhead**) in α1(II)-*Runx*2 and α1(II)-*Runx*3 mice, both of which were lacking in WT and α1(II)-*Runx*1 mice. **D,** Left, Histologic analysis of α1(II)-*Runx* mice by Safranin O staining of sections through chondrocostal cartilage, revealing the displacement of cartilage with bone marrow cavity in α1(II)-*Runx*2ΔQA mice, but not in α1(II)-*Runx*1 mice. Right, Alcian blue/alizarin red staining of skeletal preparations from α1(II)-*Runx*2ΔQA mice at 1 month of age, revealing the restricted appearance of ectopic mineralization (**arrow**).

The most striking phenotypic abnormality in the α1(II)-*Runx*3 embryos prebirth was ectopic calcification of the rib cage. In WT embryos, the frontal part of the rib cage, also called chondrocostal cartilage, never mineralized during development or throughout life, since chondrocyte hypertrophy does not occur in this cartilage. As a result, chondrocostal cartilage always stained blue in WT embryos (Figure 2C) and in adult mice. In contrast, the chondrocostal cartilage of α1(II)-*Runx*3 embryos stained red, indicating the existence of ectopic mineralization (Figure 2C, arrow). This phenotypic abnormality was identical to that observed in the α1(II)-*Runx*2 mice (Figure 2C, arrow), and reflected the presence of hypertrophic chondrocytes (7). However, the onset and extent of this phenotype was earlier and more severe in the α1(II)-*Runx*3 mice.

In contrast, neither the chondrocostal cartilage nor the chondrocranium ever stained red in α1(II)-

*Runx*1 mice at birth (Figure 2C). Consistent with the absence of ectopic red staining in the *Runx*1 mice at birth, histologic examination of the chondrocostal cartilage of these mutant mice failed to reveal any evidence of ectopic chondrocyte hypertrophy (Figure 2D). Therefore, these results indicate that the different Runx proteins each possess a distinct potential to induce ectopic chondrocyte hypertrophy, in which Runx2 and Runx3 can induce ectopic chondrocyte hypertrophy, whereas Runx1 cannot.

In addition to the ectopic endochondral mineralization observed, there was also premature endochondral ossification in other areas of the skeleton, such as the chondrocranium, in α1(II)-*Runx*3 and α1(II)-*Runx*2 mice (Figure 2C, arrowheads). In the α1(II)-*Runx*3 mice at birth, the chondrocranium stained red and the head circumferences were smaller, whereas the chondrocranium of the WT mice stained blue. In contrast, in the α1(II)-*Runx*1 mice at birth, the chondrocranium was never observed to be mineralized (Figure 2C).

The histologic findings in the growth plate of α1(II)-*Runx*1 mice were indistinguishable from those in the growth plate of WT mice at all stages analyzed, in the embryo and after birth (results not shown). Thus, Runx3 and Runx2, but not Runx1, possess the ability to accelerate the normal program of chondrocyte differentiation.

Potentiation of the ability of Runx2 to induce hypertrophic chondrocyte differentiation via the Runx2 QA domain. A unique glutamine–alanine (QA) motif is present in the amino-terminus of the runt domain of Runx2, but not in Runx1 or Runx3 (Figure 2A). In order to address the role of the QA domain in chondrocyte differentiation, we generated transgenic mice by inducing expression of a mutant form of Runx2 (11) in which the QA domain was lacking (comprising the α1(II)-*Runx*2ΔQA group of mice) (Figure 2A). Surprisingly, these mice also developed ectopic mineralization, similar to that observed in the α1(II)-*Runx*2 mice, at 1 month of age (Figure 2D), indicating that the chondrocyte differentiation ability of Runx2 does not lie solely in this domain.

Histologically, the mineralized cartilage in α1(II)-*Runx*2ΔQA mice was ectopically invaded by the bone marrow cavity (Figure 2D). However, whereas most of the male α1(II)-*Runx*2 mice died perinatally (13 of 14 transgenic mice) due to ectopic mineralization of the rib cage, none of the α1(II)-*Runx*2ΔQA mice (0 of 14 transgenic mice) died before the age of 1 month. Moreover, the extent of ectopic mineralization was significantly less severe in α1(II)-*Runx*2ΔQA mice than in α1(II)-*Runx*2 mice. These results suggest that, although the QA domain of Runx2 is not essential, it does potentiate the ability of Runx2 to differentiate chondrocytes.

Evidence of IVD degeneration in α1(II)-*Runx*1 and α1(II)-*Runx*2 mice. Since α1(II)-*Runx*1 mice had a normal lifespan, we investigated whether Runx1 plays other roles in the chondrocyte later in life. Surprisingly, starting at 3 months of age, 52% of the α1(II)-*Runx*1 mice (12 of 23 mice) developed kyphosis and scoliosis ($P < 0.01$ versus WT mice); by 6 months of age, all of the male and female α1(II)-*Runx*1 mice exhibited these features. In contrast, no such abnormalities were observed in WT mice. Radiographic evaluation revealed deformities of the vertebrae and IVD degeneration in the α1(II)-*Runx*1 mice (Figure 3A). This phenotype led us to analyze the integrity of the IVDs in these transgenic mice.

Histologic analysis showed that the IVDs of the WT mice were composed of 3 different tissue types: cartilaginous endplate of adjacent vertebrae bodies, outer annulus fibrosus, which is composed of dense, spatially oriented α1(I) collagen fibrils, and inner nucleus pulposus, a notochord remnant (21) that is mostly (80–90%) composed of water (Figure 3B). In the α1(II)-*Runx*1 mice, there was ectopic accumulation of extracellular matrix in the IVDs at ~3 months of age (Figure 3B), although the mice had not shown any abnormalities at 1 month of age (results not shown). In addition, Schmorl's node, an abnormal herniation of fibrocartilaginous tissue through the endplate and, thus, a hallmark of endplate degeneration, was also observed in α1(II)-*Runx*1 mice at 3 months of age (Figure 3D, arrow). At 6 months of age, the organized structure of the annulus fibrosus was lost, and the inner nucleus was totally replaced by extracellular matrices and had become dehydrated (Figure 3B, arrow). Also, clusters of hypertrophic chondrocytes stained positive by immunohistochemistry for α1(X) collagen (Figure 3C, arrow), although this had never been observed in the WT mice.

To determine whether this was a specific feature of Runx1 or whether other Runx proteins could also affect the integrity of the IVD later in life, we analyzed adult α1(II)-*Runx*2 mice. Similar to that observed in the α1(II)-*Runx*1 mice, the α1(II)-*Runx*2 mice that survived perinatally also developed IVD degeneration by 3 months of age (Figures 3A and B, arrow). Histologically, there was ectopic differentiation of hypertrophic chondrocytes in the IVDs of the α1(II)-*Runx*2 mice (Figure 3C, arrow), as was observed in the α1(II)-*Runx*1 mice. Collectively, these results indicate that when the Runx proteins are overexpressed, they can affect IVD integrity.

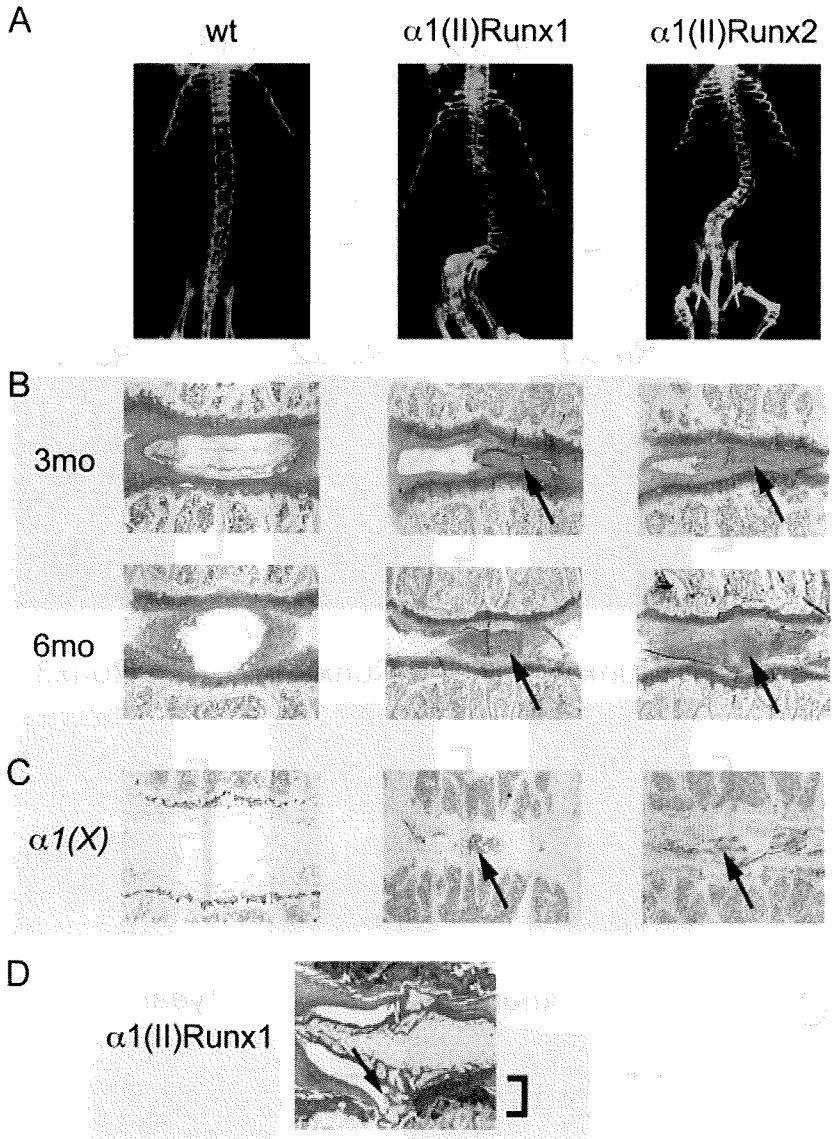

Figure 3. Intervertebral disc (IVD) degeneration in α1(II)-*Runx*1 and α1(II)-*Runx*2 mice. **A,** Radiographic analysis of the vertebrae at 3 months revealed marked scoliosis in the IVDs of α1(II)-*Runx* mice as compared with wild-type (WT) mice. **B–D,** Coronally cut sections of the IVDs, along with adjacent vertebral bodies, were assessed histologically by Safranin O staining (**B** and **D**), and by immunohistochemistry (**C**), which showed ectopic α1(X) collagen expression. Note the progressive degeneration of the IVDs and displacement by extracellular matrix in the α1(II)-*Runx*1 and α1(II)-*Runx*2 mice **(arrow)** (**B** and **C**), and the protrusion of the IVD **(arrow)** through the endplate into the columnar growth plate **(bracket)** in α1(II)-*Runx*1 mice **(D)**.

Induction of *Runx* gene expression in the cartilaginous endplate following weight loading. The fact that there were phenotypic abnormalities in adult α1(II)-*Runx*1 and α1(II)-*Runx*2 mice suggested that the Runx proteins may have an as yet unappreciated function in the IVD. To address this question, we first analyzed the expression of *Runx* genes in IVDs during embryonic development. At embryonic day 16.5, all of the *Runx* genes were expressed in specific regions of the vertebral body and/or the IVD (Figure 4A). *Runx*1 was mainly expressed in the primary ossification center. *Runx*2 was also expressed in the ossification center, in chondrocytes and cells surrounding the prospective IVD. *Runx*3 was specifically expressed in prehypertrophic chondrocytes.

We also analyzed the expression of each Runx protein by immunohistochemistry, which revealed identical patterns of expression between the 3 proteins

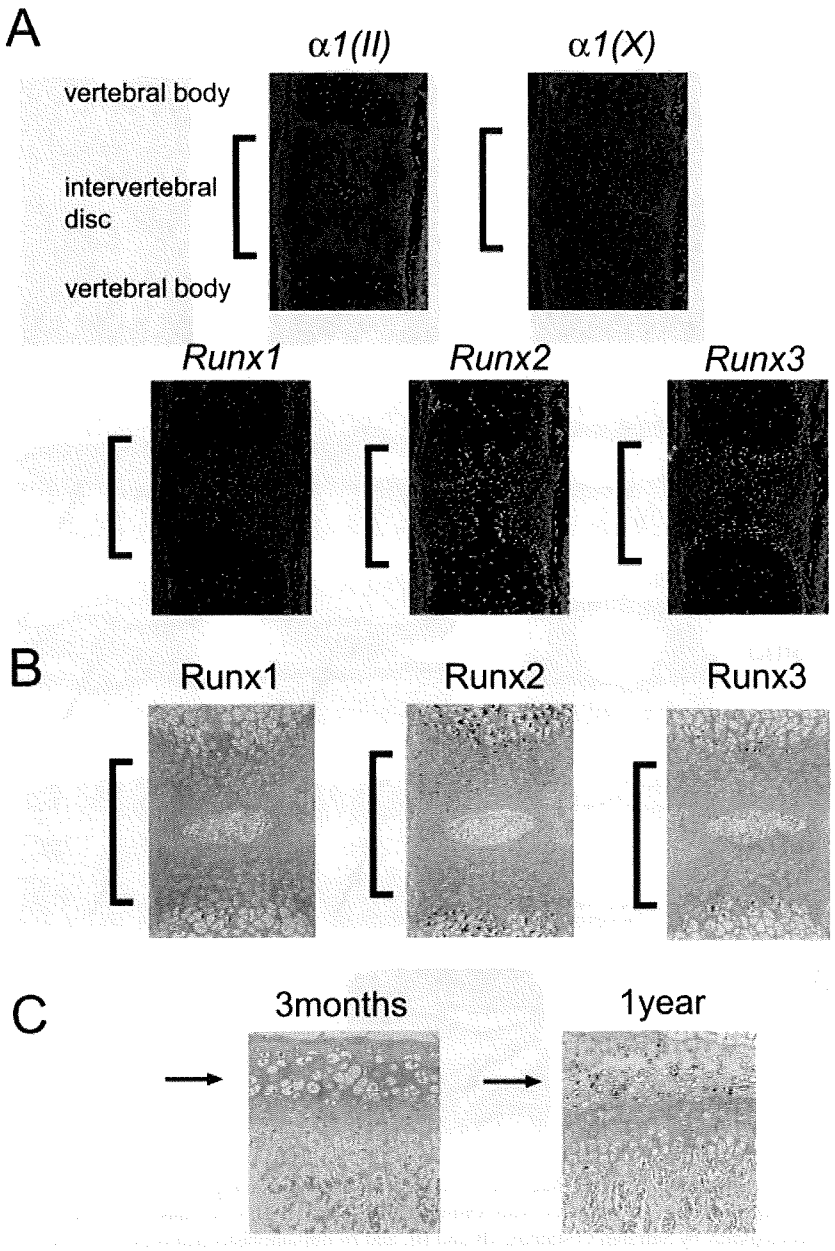

Figure 4. Expression of *Runx*2 in intervertebral discs (IVDs). Adjacent sections of wild-type mouse embryos at embronic day 16.5 were assessed by in situ hybridization using the indicated probes **(A)**, and by immunohistochemical analysis **(B** and **C)**. Note the expression of *Runx*2 in the prospective IVD **(bracket)** (**A** and **B**). Immunohistochemical analysis of the IVDs after birth revealed that *Runx*2 was not expressed in the wild-type mice at 3 months of age, but was expressed at 1 year **(arrow)** (**C**).

(Figure 4B). These analyses showed that Runx2 was the only member of the family that was physiologically expressed in the prospective IVD.

We next analyzed *Runx*2 expression in the IVDs of WT mice after birth. Whereas the expression of *Runx*2 in the IVDs was close to background values at 1 month and 3 months of age (results not shown and Figure 4C), it had increased in the endplate of the IVDs of WT mice at 1 year (Figure 4C, arrow).

Since the overexpression of *Runx*1 or *Runx*2 led to degeneration of the IVD, and Runx2 protein was detected in the IVD, we tested whether *Runx*1 or *Runx*2 induces IVD degradation in pathologic conditions. To test this possibility, we analyzed the biomechanical func-

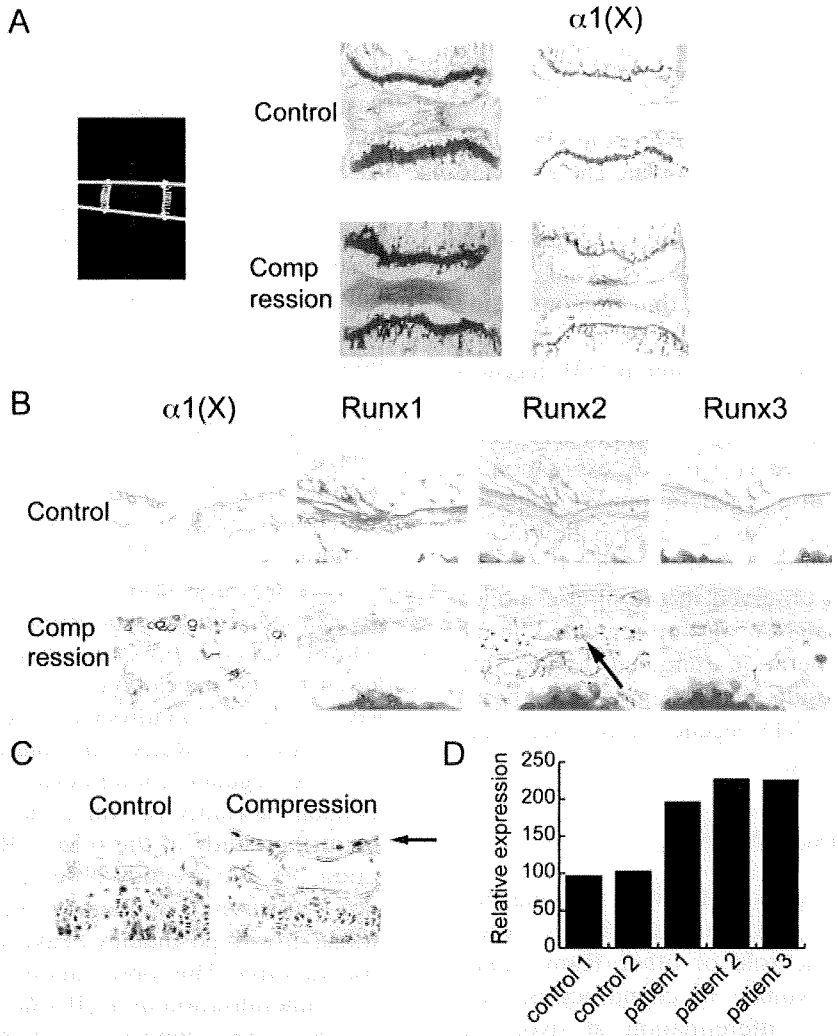

Figure 5. Evaluation of intervertebral disc (IVD) degeneration in mice and humans. **A,** Induction of *Runx*2 expression by mechanical compression in a mouse model of IVD degeneration. Caudal vertebrae from 2-month-old wild-type mice were compressed by an elastic spring, and then assessed by radiography (left), histology (middle), and immunohistochemistry (with Safranin O staining) (right). The compressed IVDs showed degeneration and ectopic α1(X) collagen expression (right). **B,** Immunohistochemical analysis of the expression of Runx proteins in adjacent sections of the compressed vertebrae. Note the specific induction of Runx2 in the endplate of the compressed vertebrae **(arrow)**, with coexpression of α1(X) collagen. **C,** Induction of *Runx*2 mRNA expression by compression. Vertebrae from *Runx*2$^{+/-}$ mice were compressed and analyzed by LacZ staining. Note the specific induction of *Runx*2 mRNA in the endplate **(arrow)**. **D,** Up-regulation of *Runx*2 in human patients with IVD degeneration. Quantitative polymerase chain reaction showed that *Runx*2 expression was significantly up-regulated in patients with IVD degeneration compared with unaffected control subjects.

tion of the IVDs of WT mice in a model of mechanical stress–induced compression, the most frequent cause of IVD degeneration. For this test, we transfixed the vertebral body with steel wire and instrumenting elastics for 4 weeks (Figure 5A), and compared Runx protein accumulation before and after compression.

After compression of the IVDs, typical disc degeneration was observed, in the form of a damaged endplate and massive induction of cells positive for type X collagen, which indicated the appearance of hypertrophic chondrocytes (Figure 5A). *Runx*1 expression was undetectable before and after compression (Figure 5B), suggesting that *Runx*1 does not contribute to IVD degeneration under these conditions. *Runx*3 expression was observed after compression, albeit at a very low level (Figure 5B). In sharp contrast, there was strong induction of Runx2 protein expression in the endplate after compression (Figure 5B, arrow). Moreover, cells expressing Runx2 also expressed α1(X) collagen, indicative of the appearance of hypertrophic chondrocytes (Figure 5B).